2-20-2019

Testing pyroxenite versus peridotite sources for marine basalts using U-series isotopes

Lynne J. Elkins

Bernard Bourdon

Sarah Lambart

Lithos 332–333 (2019) 226–244

Contents lists available at ScienceDirect

Lithos

journal homepage: www.elsevier.com/locate/lithos

Invited review article

Testing pyroxenite versus peridotite sources for marine basalts using U-series isotopes

Lynne J. Elkins [a,*], Bernard Bourdon [b], Sarah Lambart [c]

[a] University of Nebraska-Lincoln, Lincoln, NE, USA
[b] Ecole Normale Supérieure de Lyon, CNRS, UCBL, Université de Lyon, Lyon, France
[c] University of Utah, Salt Lake City, UT, USA

ARTICLE INFO

Article history:
Received 24 September 2018
Accepted 16 February 2019
Available online 20 February 2019

ABSTRACT

Geochemically enriched signatures in global oceanic basalts have long indicated a heterogeneous mantle source, but the role of lithologic heterogeneity in producing mantle partial melts, particularly fertile pyroxenite rocks, remains unclear. Uranium-series disequilibria in basalts are particularly sensitive to the increased garnet mode and melting rates of pyroxenite rocks, making the system a useful indicator of mantle lithologic heterogeneity in the melt region for oceanic basalts. Here we summarize evidence for the presence and importance of pyroxenite rocks in the upper mantle and their role in melt generation of mid-ocean ridge basalts and ocean island basalts, with a synthesis of U-series disequilibrium systematics in oceanic basalts and implications for global lithologic heterogeneity of the upper mantle. We further synthesize the melt modeling approaches for the interpretation of U-series disequilibria in basalts and demonstrate the use of numerical solution models for time-dependent reactive porous flow and dynamic melting during decompression of a two-lithology mantle in thermal equilibrium. Our model outcomes corroborate prior interpretations in favor of reactive porous flow and two-porosity transport for relatively homogeneous, peridotite-dominated mantle regimes, and further support contributions of pyroxenite partial melts to aggregated melts in order to reproduce the heterogeneous global basalt data. To most accurately predict the conditions of melting by comparison with measured data, two-lithology melting calculations should carefully consider the role of thermal equilibrium, mineral/melt partitioning, non-linear variations in mineral modes, and degree of melting during the melting process.

Contents

* Corresponding author.
E-mail address: lelkins@unl.edu (L.J. Elkins).

https://doi.org/10.1016/j.lithos.2019.02.011
0024-4937/

1. Introduction

The lithologic makeup of the Earth's mantle remains a fundamental question in geoscience, with major implications for chemical planetary evolution and the nature of chemical exchanges and dynamic forcings between the mantle and the crust. Lithologic heterogeneity in the mantle, especially the presence of mafic lithologies such as eclogite and pyroxenite, could play an important role in the generation of basaltic ocean crust at both divergent tectonic settings and oceanic hotspots, which together constitute the overwhelming majority of magmatic and volcanic activity on Earth (e.g., Allègre et al., 1984; Chase, 1981; Hirschmann and Stolper, 1996; Hofmann, 1997; Zindler et al., 1984). Understanding the nature and role of those heterogeneities is thus crucial for achieving a greater understanding of mantle dynamics, mantle chemical evolution, oceanic crust genesis, and plate tectonics.

Much has been accomplished since Allègre and Condomines (1982) proposed that U-series isotopes could be used to detect the influence of mafic mantle lithologies on the generation of oceanic basalts (e.g., Elkins et al., 2016; Koornneef et al., 2012; Prytulak et al., 2014; Prytulak and Elliott, 2009; Russo et al., 2009; Turner et al., 2015; Waters et al., 2011). These developments are largely owed to the particular sensitivity of U-series isotope systems to garnet mode and mantle fertility, both effective tracers of source lithology (e.g., Elkins et al., 2014, 2016; Hirschmann and Stolper, 1996; Koornneef et al., 2012; Pertermann and Hirschmann, 2003a; Prytulak and Elliott, 2009). The technique has been particularly effective when coupled with major element, trace element, and/or radiogenic isotope data, which help to identify long-lived compositional variations in the mantle domain (e.g., Elkins et al., 2014, 2016; Koornneef et al., 2012; Prytulak and Elliott, 2009; Waters et al., 2011). While there are limitations to the U-series disequilibrium technique, the current state of study is encouraging and suggests a promising avenue forward for investigating lithologic heterogeneity in the mantle source of recently erupted oceanic basalts. On the whole, results from U-series isotope measurements and modeling broadly support the presence and important melting role of pyroxenite in the sub-oceanic mantle.

This paper discusses our current understanding of U-series detection of lithologic source heterogeneity in oceanic basalts, with an aim to review and synthesize the developments of recent decades, and to offer suggestions for future directions in the study of mantle lithologic heterogeneity and its implications. The specific questions addressed by this review are two-fold: 1) how are U-series isotopes a useful tool for investigating the nature and magnitude of mantle lithologic heterogeneity? and 2) how has this technique helped our understanding of mantle makeup and melt generation processes to date, and where might the geochemical community best concentrate its future efforts? Below, we address these questions through a synthesis of recent research, including a fresh look at lithologically-focused melting models to interpret U-series geochemical data.

Due to our primary focus on mantle lithologies and to limit the scope of this review, we do not address the possible impacts of volatile content on melting and U-series isotopes here, and the reader is referred to studies that have considered this question for further analysis (e.g., Asimow et al., 2004; Bourdon et al., 1996a, 2005, 2006; Reagan et al., 2017; Turner et al., 1997). Likewise, we focus on lithologies contributing to partial melting and basalt genesis, and do not address what nonetheless clearly constitutes an important dimension of mantle heterogeneity and of the chemical evolution of the mantle, namely refractory lithologies such as dunites and harzburgites (Rampone and Hofmann, 2012; Warren, 2016, and references therein).

2. A lithologically heterogeneous mantle

2.1. The nature of mantle heterogeneity

Studies of mid-ocean ridge and hotspot volcanism have long called for heterogeneous source regions (Hofmann, 1997, 2007, and references therein). While the presence of chemical heterogeneity is not contested, ongoing debate has centered on the lithologic hosts for this heterogeneity in the mantle (e.g., Chazot et al., 2005; Constantin et al., 1995; Dantas et al., 2007; Hébert et al., 2001; Hirschmann and Stolper, 1996; Kempton and Stephens, 1997; Rampone and Borghini, 2008; van Acken et al., 2008; Warren et al., 2009). The two main schools of thought suggest that: (1) chemical heterogeneity is hosted in olivine-poor, pyroxene-rich mafic lithologies, i.e. "pyroxenites" (e.g., Hirschmann and Stolper, 1996), which, based on lithological proportions in orogenic massifs, may constitute 2 to 5% of the Earth's upper mantle; or (2) chemical heterogeneity is hosted in (metasomatized) peridotites and no lithological heterogeneity is required (e.g., Prytulak and Elliott, 2009; Stracke et al., 1999).

The large compositional variability of pyroxenites in both major and trace elements obscures how influential these lithological heterogeneities can be in generating oceanic basalts, contributing to the ongoing debate. Pyroxenites range from basaltic to ultramafic compositions (Kogiso et al., 2004a, Lambart et al., 2013) and present rare earth element (REE) patterns either broadly parallel to normal MORB or exhibiting strong fractionation, with low HREE concentrations and/or significant LREE-enrichment (Downes, 2007). Radiogenic isotope signatures of observed mantle pyroxenites likewise extend towards multiple mantle end-members, suggesting diverse origins (e.g., Day et al., 2009; Medaris et al., 1995; Varas-Reus et al., 2018; Xu, 2002).

The potential presence of diverse mantle lithologies has broad implications for the chemical evolution of the Earth's mantle. In the simplest scenarios, pyroxenites are inferred to originate by plate tectonic recycling: subducted crust enters the convecting mantle, metamorphoses to high-density eclogite rock, and is eventually returned to the shallow upper mantle by mantle convection or deep-seated mantle plumes, either as upwelling "plums" or mechanically stirred veins (e.g., Halliday et al., 1995; Kellogg and Turcotte, 1990; Phipps Morgan, 2001; van Keken et al., 2002; White and Hofmann, 1982). More refined models incorporate subduction recycling of the underlying oceanic lithosphere (Kerr et al., 1995), consider more diverse subducted lithologies (e.g., Herzberg, 2010), and evaluate the chemical changes rocks may experience during subduction, such as dehydration reactions and fluid loss (e.g., Kogiso et al., 2003) or early melting events (e.g., McDonough, 1991). Delamination of underplated continental basalts can also act as an additional source of mafic rocks in the mantle (e.g., Elkins-Tanton and Foulger, 2005; Jull and Kelemen, 2001; Kay and Kay, 1993; Lee and Anderson, 2015). This complex set of scenarios underscores the importance and likelihood of a highly heterogeneous source. Empirical

(e.g., Brunelli et al., 2005; Dick et al., 2010; Godard et al., 2008; Hellebrand et al., 2002; Seyler et al., 2007) and experimental (e.g., Lambart et al., 2012; Lundstrom et al., 2000; Sobolev et al., 2007; Yaxley and Green, 1998) observations further suggest that additional processes (mechanical mixing, chemical hybridization, melt impregnation, or melt metasomatism) may generate and modify pyroxenites in the mantle, leading to predictions for additional variability in the mantle source. Such sources further complicate our picture of the mantle, and it remains unclear how important this degree of heterogeneity would be during melting and mixing of melts from a broad mantle zone.

2.2. Partial melting in a lithologically heterogeneous mantle

The debate around the role of mantle pyroxenite in generating oceanic basalts centers on determining the degree to which the presence of a small amount of fusible lithology impacts the quantity and composition of resulting partial melts under typical mantle conditions. Since the 2000s, numerous experimental studies have investigated the melting behavior of pyroxenite in an effort to address this question (Lambart et al., 2013, and references therein). Notably, most pyroxenite compositions referenced in the literature have lower solidus temperatures and shorter melting intervals (i.e., the difference in temperature between solidus and liquidus) than those of peridotite rocks: approximately 75% of observed pyroxenite compositions have solidus temperatures as much as 50-150°C below those of peridotites in the mantle, and melting intervals range from ~150°C in some pyroxenites to as much as 400-500°C in peridotite rocks (Hirschmann and Stolper, 1996; Lambart et al., 2016). As a result, pyroxenite melting is expected to initiate deeper and be more productive than peridotite melting under similar conditions, and thus to have a disproportionate impact on the compositions of basalts (e.g., Hirschmann and Stolper, 1996; Sleep, 1984). A small pyroxenite fraction within an ambient peridotitic mantle also experiences enhanced melting due to heat exchange below the peridotite solidus (e.g., Hirschmann and Stolper, 1996; Phipps Morgan, 2001; Sleep, 1984; Stolper and Asimow, 2007; Stracke and Bourdon, 2009), further reinforcing the impact of pyroxenite melting. To further complicate matters, solidus depths and melting intervals, as well as the chemical compositions of resulting partial melts, are potentially affected by the composition and mineralogy of the source rock, including garnet mode, alkali and Ti contents, Mg number, and vacancies in clinopyroxene (Kogiso et al., 2004a; Lambart et al., 2016; Pertermann and Hirschmann, 2003a; Rosenthal et al., 2014, 2018). In particular, pyroxenite partial melts are expected to have high Fe and Ti contents, highly variable CaO/Al_2O_3 ratios and SiO_2 contents, and distinct trace element ratios (Ba/Th, La/Nb, Sr/Nd) compared to peridotite partial melts (Hirschmann et al., 2003; Kogiso et al., 2003, 2004a; Lambart et al., 2009, 2013; Prytulak and Elliott, 2007; Spandler et al., 2017; Stracke and Bourdon, 2009).

Predicting the outcomes of pyroxenite melting relies on accurate calculations for those processes, but forward melt model calculations of decompression melting in a heterogeneous mantle must also assume a particular melting regime. The two most common scenarios for geochemical models in the literature consider each lithology either in both thermal and chemical isolation (e.g., Koornneef et al., 2012; Natland, 1989; Prinzhofer et al., 1989; Zhang et al., 2012) or in thermal equilibrium, but chemically isolated (e.g., Borghini et al., 2017; Brunelli et al., 2018; Hirschmann and Stolper, 1996; Rudge et al., 2013; Sims et al., 2013), two scenarios that can be expressed in terms of length-scale of the heterogeneity. The case of thermal isolation corresponds to the presence of a large-scale heterogeneity (>10 km), consistent with some geophysical observations (e.g., Ishii and Tromp, 1999; Kaneshima and Helffrich, 1999), while the thermal equilibrium case corresponds to shorter length scales (kilometer-sized or smaller), consistent with several recent studies (e.g., Harvey et al., 2006; Liu et al., 2008; Liu and Liang, 2017; Shorttle and Maclennan, 2011; Warren and Shirey, 2012).

For the thermal equilibrium scenario, energy exchange has been typically approximated by assuming a thermal regime in which the pressure-temperature path is controlled by adiabatic melting of the dominant peridotite rocks (e.g., Hirschmann and Stolper, 1996; Lambart et al., 2009). Recently, Lambart (2017) instead considered the effects of full thermal energy exchange between pyroxenite and peridotite source rocks using Phipps-Morgan's (2001) model for energy exchange between lithologies, together with Lambart et al.'s (2016) parameterization of pyroxenite experimental outcomes to assess pyroxenite melt fractions. Much like predictions by Hirschmann and Stolper (1996), Pertermann and Hirschmann (2003a), and others, Lambart's (2017) approach illustrated that prior to peridotite melting, pyroxenites with deeper solidi follow a superadiabatic pressure-temperature path because they draw heat from the ambient peridotite. A key difference in the outcomes of melting with full thermal exchange is the slowing or stopping of pyroxenite melting when the peridotite solidus is reached, due to the shallower P/T slope of the pyroxenite solidus than that of the peridotite rocks; this effect is enhanced when larger quantities of pyroxenite are present. This outcome agrees with predictions by Sobolev et al. (2005) and Phipps Morgan (2001) that, contrary to previous assumptions, pyroxenites may not fully melt during mantle upwelling. The revised melting paths produce significant differences in trace element compositions for mixtures of melts derived from the two lithologies (Lambart, 2017).

Beyond the most simple melt modeling outcomes, the mode of melt transport and extraction in a multi-lithologic mantle may further impact the composition of erupted basalts (e.g., Ito and Mahoney, 2005a; Ito and Mahoney, 2005b; Stracke and Bourdon, 2009, and references therein). Indeed, evidence from Os isotopes suggests the participation of mafic lithologies in oceanic basalt genesis (e.g., Hauri and Hart, 1993; Lassiter et al., 2000; Schiano et al., 1997), but importantly, melting of pyroxenite to produce oceanic basalts may require rapid transport of magma from the source to the surface in order to preserve the radiogenic signature of the pyroxenite (Kogiso et al., 2004b). With rapid transport, heterogeneities as small as 0.1 to 1 m in diameter may be sufficiently large to segregate partial melts without reequilibrating or freezing (Kogiso et al., 2004b) and thus may impact final basalt compositions significantly. Recent energy-constrained modeling calculations (Hewitt, 2010; Katz and Weatherley, 2012; Weatherley and Katz, 2012) have further advanced previous suggestions that lithologic heterogeneity in a melting regime may produce reaction infiltration instabilities leading to channelized flow (e.g., Aharonov et al., 1997; Daines and Kohlstedt, 1994; Kelemen et al., 1997; Spiegelman et al., 2001), which in turn would influence magma mixing, basalt compositions, and the efficiency of melt extraction, making such heterogeneities potentially highly consequential to mantle and crustal dynamics. Weatherley and Katz (2012), in particular, observed that over a wide range of parameters, lithologic heterogeneity consistently causes high-porosity channels to form in the upwelling mantle, strongly influencing magma transport dynamics. Further tests by Weatherley and Katz (2016) have confirmed that channel formation appears robust for different sizes, shapes, abundances, distributions, and compositional ranges of fusible heterogeneities. In their models, channels form immediately after crossing the solidus of the lower productivity, ambient peridotite rocks (Weatherley and Katz, 2016), in good agreement with previous expectations (Lundstrom, 2000; Mallik and Dasgupta, 2012; Spiegelman and Kelemen, 2003); the channels are thereafter protected by cool sheaths that maintain channel stability throughout the melt zone (Pertermann and Hirschmann, 2003a; Weatherley and Katz, 2012). If correct, the findings summarized above would support a key and central role for pyroxenite in producing oceanic crust through its influence on melt generation and magma transport processes.

2.3. Constraints on mantle lithologies from basalt geochemistry

The compositions of oceanic basalts themselves provide important clues to the nature of the mantle melt source, but as basalts represent

mixtures of melts from a complex and potentially large melting regime, interpreting their chemistry requires careful analysis, and work to-date has provided conflicting results. The major element, trace element, and radiogenic isotope compositions of oceanic basalts have previously been studied to investigate the presence and importance of lithological heterogeneities in the upper mantle (e.g., Hirschmann et al., 2003; Le Roux et al., 2002; Shorttle et al., 2014; Stracke and Bourdon, 2009). For major element compositions, these interpretations have, in part, been premised on comparisons of basalt compositions with experimental results for peridotite and pyroxenite melting under mantle temperature and pressure conditions. Low CaO and high SiO_2 and NiO contents of Hawaiian tholeiites have been interpreted to indicate partial melt contributions from hybrid secondary pyroxenite (Herzberg, 2006; Sobolev et al., 2005), i.e., olivine-free garnet pyroxenite formed through the chemical reaction of eclogite-derived partial melts with peridotite rocks (Sobolev et al., 2005; Yaxley and Green, 1998). Partial melts derived from silica-deficient pyroxenites are less silicic and more alkaline than peridotite melts (Hirschmann et al., 2003; Kogiso et al., 2003; Lambart et al., 2009), leading Hirschmann et al. (2003) to further suggest that silica-deficient pyroxenite may contribute to the genesis of alkali basalts from ocean island settings. Low SiO_2 concentrations coupled with high FeO contents in MORB have also been suggested as indicators of pyroxenite in the mantle source (Lambart et al., 2009, 2013).

Transition element (e.g., Ti, Mn, Fe, Co, Ni, Zn) concentrations in magmas have been recently used as additional indicators of mantle source mineralogy (e.g., Davis et al., 2013; Herzberg, 2010; Humayun et al., 2004; Le Roux et al., 2010, 2011; Prytulak and Elliott, 2007; Qin and Humayun, 2008; Sobolev et al., 2005, 2007), though the reliability of this approach is debated (Matzen et al., 2017). Experimental partition coefficients for pyroxenitic compositions have also shown that the mineral compositions themselves, especially clinopyroxene and garnet, can affect the major and trace element composition of partial melts (e.g., Elkins et al., 2008; Pertermann and Hirschmann, 2003a; Spandler et al., 2017). Finally, Ba/Th, La/Nb, Sr/Nd, Ba/Ta, Nb/Zr, rare earth element ratios, TiO_2 contents, Hf isotope ratios and other geochemical indicators have been invoked to suggest the presence (or absence) of pyroxenite in the melt regime for a number of locations, such as the Azores, Hawaii, and Iceland (e.g., Hofmann and White, 1982; Lassiter et al., 2000; Phillips et al., 2016; Prytulak and Elliott, 2007; Salters and Dick, 2002; Shorttle et al., 2014; Stracke and Bourdon, 2009).

It is typically expected that pyroxenite-derived melts present incompatible element enrichment, as well as time-integrated long-lived radiogenic isotope signatures of such enrichment (e.g., high $^{87}Sr/^{86}Sr$ and $^{187}Os/^{186}Os$ and low $^{143}Nd/^{144}Nd$ and $^{176}Hf/^{177}Hf$ ratios) (Blichert-Toft et al., 1999; Millet et al., 2008; Salters and Dick, 2002; Schiano et al., 1997; Sobolev et al., 2008). For this reason, the contribution of of mantle pyroxenite in the melt regime is generally expected to correlate with some enrichment in radiogenic isotope signatures. However, a number of studies have demonstrated that partial melting of a heterogeneous mantle, variations in melt transport, and magma chamber processes may either fail to produce or actively obscure straightforward patterns of basalt geochemistry (e.g., Coogan and O'Hara, 2015; Lissenberg et al., 2013; Lissenberg and MacLeod, 2016; Maclennan, 2008; O'Hara, 1977; Rubin et al., 2009; Rudge et al., 2013). Melt flow variations (e.g., Spiegelman and Kelemen, 2003), melt-rock reaction (Lissenberg et al., 2013), and magma mixing can also create significant variability in trace element abundances in basalt. Importantly, Rudge et al. (2013) demonstrated that isotopic trends defined by oceanic lavas do not necessarily point directly toward the isotopic ratio of the mantle source. Magma chamber processes can also obscure primary basalt geochemistry (Maclennan, 2008; Rubin et al., 2009; Rudge et al., 2013), and open-system magma chamber cycling could significantly affect the trace element composition of mantle-derived basalts (O'Neill and Jenner, 2012). These complications with the method of using the geochemical compositions of basalts to identify heterogeneity in the melt regime are further compounded by ambiguity concerning the true host lithology that is associated with trace element and isotopic enrichment; by potentially large variations in the ages of source components and resulting impacts on radiogenic isotopic ingrowth (e.g., Lambart, 2017; Stracke et al., 2003a); and by the significant range of potential types of pyroxenite and associated residual minerals during the melting process (and resulting effects on melting behavior) (Lambart et al., 2016). As a result, the true role of pyroxenite in generating oceanic basalts continues to be contested.

While subject to its own limitations, as explored below, the addition of U-series isotopic disequilibrium analysis to the arsenal of geochemical tools has proven useful, as the system is particularly sensitive to melt productivity and its impact on melting rate, rather than principally to source compositions. Where young, fresh basalts are available, U-series disequilibrium data have, at least in some cases, fingerprinted rapid melting due to enhanced source fertility, suggesting the presence of pyroxenite in the melt source (e.g., Elkins et al., 2014, 2016; Koornneef et al., 2012; Prytulak and Elliott, 2009; Russo et al., 2009; Waters et al., 2011).

3. Principles of U-series disequilibria in partial melting regimes

The U-series decay system consists of radioactive nuclides that decay from one of three initial parents (^{238}U, ^{235}U, or ^{232}Th) to ultimately stable daughter radionuclides (^{206}Pb, ^{207}Pb, and ^{208}Pb) via a series of intermediate radioactive daughters with a range of half-lives (Fig. S1). In the absence of a perturbation, the U-series isotope decay chain reaches a state of secular equilibrium where all the nuclide activities ($=\lambda N$) are equal. Chemical fractionations between elements such as U, Th, or Pa disrupt secular equilibrium, leading to an excess or deficit of a given nuclide relative to equilibrium. It takes approximately five half-lives of the shorter-lived daughter nuclide for the system to again reach secular equilibrium. This isotopic disequilibrium is measured using activity ratios such as ($^{230}Th/^{238}U$) and ($^{231}Pa/^{235}U$). The system is sensitive not only to the magnitude and sense of chemical fractionations, such as those that occur during partial melting, but also to the timescales over which such fractionations occur, which are controlled by factors such as melt fertility, porosity, and permeability effects on melt transport, and solid mantle upwelling rates (e.g., McKenzie, 1985; Spiegelman and Elliott, 1993; Williams and Gill, 1989). Uranium-series studies of melting and melt extraction have particularly focused on disequilibria between the nuclides ^{238}U-^{230}Th-^{226}Ra and ^{235}U-^{231}Pa, because their half-lives are particularly relevant to the timescales of melting and melt transport (e.g., Bourdon et al., 2003). The reader is referred to Fig. S1, and to the summary by Bourdon et al. (2003) and references therein for further information about U-series isotope radioactive decay and the basic equations governing secular equilibrium and nuclide behavior.

As discussed above, major element, trace element, and radiogenic isotope compositions of oceanic basalts have long indicated a heterogeneous mantle source, but the lithologic nature of that source has been unclear. Uranium-series isotopes have proven to be advantageous in this regard, due to their great sensitivity to lithologic type and melting rates.

3.1. Overview of magma generation and transport effects on U-series isotopes

Because the U-series nuclides are all highly incompatible, they mostly fractionate from each other only at very small degrees of melting (<1%). Uranium is, however, less incompatible than Th in garnet; hence, the presence of garnet during melting generates elevated ($^{230}Th/^{238}U$) activity ratios (> 1) in partial melts and makes isotopic disequilibrium between ^{230}Th and ^{238}U a sensitive indicator of garnet in the source residue (e.g., Beattie, 1993; Blundy and Wood, 2003; Elkins et al., 2008; Hauri et al., 1994b; La Tourette et al., 1993). In the absence of garnet, clinopyroxene largely controls U and Th partitioning

in typical mantle rocks. While aluminous clinopyroxene found in peridotites at pressures approaching the garnet stability field can have $D_U/D_{Th} > 1$, garnet-free lithologies dominantly produce melts with lower ($^{230}Th/^{238}U$) (≤ 1) (e.g., Blundy and Wood, 2003, and references therein). As a result, ($^{230}Th/^{238}U$) ratios are sensitive to the mineralogic makeup and lithology of the source rock for basaltic partial melts, and thus can provide information about the lithologies present in basaltic melt sources.

Early research also identified a possible relationship between ($^{230}Th/^{232}Th$) activity ratios, $^{87}Sr/^{86}Sr$ ratios, and Th/U ratios (e.g., Allègre and Condomines, 1982; Ben Othman and Allègre, 1990; Chabaux and Allègre, 1994; Condomines et al., 1981), thought to reflect source heterogeneity. A larger and more precise global data set, together with melting models that account for the long residence time of U in the melting residue (e.g., Williams and Gill, 1989) have demonstrated that ($^{230}Th/^{232}Th$) variations in oceanic basalts can be produced without necessarily requiring source heterogeneity, due to the accumulated effects of melting gradually over time, thereby adding complexity to investigations of source type. This possibility must be addressed if the U-series disequilibrium method is to be used to effectively address source lithology questions. Here we briefly explore inferences drawn from melting models regarding the generation of partial melts by a homogeneous source, in order to better fingerprint indicators of mantle heterogeneity. The reader is referred to the Supplementary Information for additional summaries of these models.

The "dynamic melting" models of McKenzie (1985) and Williams and Gill (1989) considered radioactive decay and ingrowth within the U-series decay chains, where partial melting occurs in a near-fractional scenario with a fixed matrix porosity (Fig. 1a). In such a model, melting takes place during decompression in a vertical section of upwelling mantle (Fig. 1a). Uranium-series disequilibria arise when parent and daughter nuclides have different residence times in the melting column, i.e., when their bulk partition coefficients are different during instantaneous partial melting, such as in the presence of residual garnet (e.g., Blundy and Wood, 2003). The extent of U-Th disequilibrium in the aggregated melt is thus sensitive to both the source mineralogy, particularly the garnet mode, and the overall melting rate. Hence, ^{238}U-^{230}Th disequilibrium can be created by partial melting of a homogeneous mantle source, with the largest ^{230}Th excesses produced by slow upwelling (corresponding to low melting rate) in the garnet stability field and by the deepest onset of melting (i.e., highest mantle potential temperature) (e.g., Elliott, 1997; Sims et al., 1999). However, to preserve the U-series disequilibria observed in basalts (see Section 4), dynamic melting must also correspond to rapid, channelized transport of melts, without further exchange with unmelted rock material after magma segregation.

Spiegelman and Elliott (1993) suggested an alternative model where chemical equilibrium is continuously achieved throughout the process of melt production and migration through a permeable, porous rock matrix (Fig. 1b). Their model, which we refer to as "reactive porous flow" (RPF) melting, resembles chromatographic melt transport scenarios (e.g., Bickle and McKenzie, 1987; Navon and Stolper, 1987; Ribe, 1985), envisioned as a percolating, capillary-like network with slow travel times and sufficient opportunity for equilibrium melt-rock chemical interactions to occur, producing chromatographic effects. Their model also incorporates residence time effects on the ingrowth of continuously fractionating U-series nuclides. Notably, RPF models alleviate the most extreme transport rate requirements imposed by dynamic melting models. Because RPF melting produces significant isotopic disequilibrium throughout the melting process, even to very shallow depths, it presents an alternative explanation for high ($^{226}Ra/^{230}Th$) ratios observed in basalts (e.g., Lundstrom et al., 1995; Sims et al., 2002; Spiegelman and Elliott, 1993).

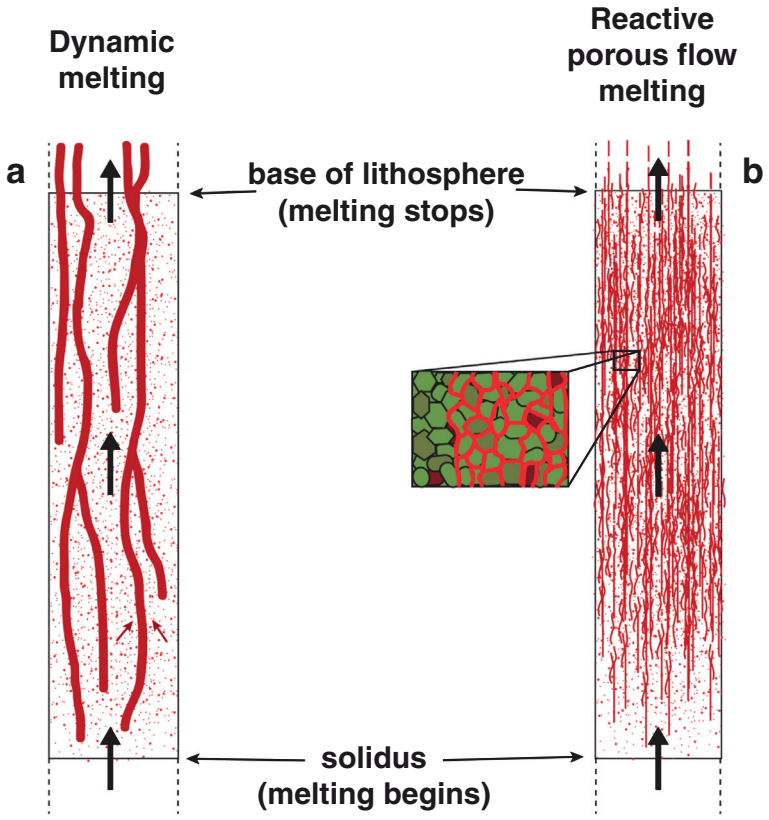

Fig. 1. Conceptual diagram illustrating time-dependent melting scenarios for an upwelling mantle column experiencing a. dynamic melting and b. RPF processes (after McKenzie, 1985; Spiegelman and Elliott, 1993; Williams and Gill, 1989). Red specks indicate small degrees of melt residing in the pore space of the host rock, while red lines and black arrows indicate magma flow paths. Flow paths for dynamic melting are illustrated with thick red lines to indicate the presence of high-porosity, dunite channels of some finite width, while RPF flow paths follow low-porosity grain boundaries.

The two models thus explore opposing extremes of chemical interaction (complete equilibrium for the former and disequilibrium during transport for the latter), with different implications for the nature of mantle melting, melt transport, and dynamics. A number of researchers have suggested that the natural mantle environment is likely a combination or intermediate between these mechanistic extremes (e.g., Jull et al., 2002; Sims et al., 2002; Spiegelman and Kenyon, 1992; Weatherley and Katz, 2012, 2016), and the two model scenarios thus present a useful framework for modeling and understanding mantle behavior and the generation of oceanic crust.

While the dynamic and RPF models focus on melting of homogeneous peridotitic mantle, considering and understanding their usage is critical to investigating questions about heterogeneous source melting and its effects on U-series isotope disequilibria, as explored further below.

3.2. Effects of mantle heterogeneity on U-series isotopes

The modeling efforts summarized above focused on the effects of melting an initially homogeneous mantle source that experiences progressive melt depletion effects, thereby generating a heterogeneous source during melting (after e.g., Goldstein et al., 1991; Rubin and Macdougall, 1992; Williams and Gill, 1989). However, the mantle producing oceanic basalts is itself geochemically and lithologically heterogeneous prior to the inception of melting, and mantle pyroxenite rocks have been directly invoked to account for U-series disequilibria in basalts in numerous other settings. For instance, Lundstrom et al. (1998b) specifically invoked the effects of heterogeneous source melting and mixing for MORB, but did not consider lithologic effects on the melting process – largely because the melting behavior of mafic lithologies under mantle conditions were, at the time, poorly constrained. Lundstrom et al. (1999) also invoked melt fertility variations to explain the formation of channels by reactive infiltration instabilities and to predict their impacts on U-series disequilibria. Waters et al. (2011) further suggested that, in some cases, the U-series isotopic data arrays observed in mid-ocean ridge basalts require both progressive melt depletion with differential transport and source heterogeneity effects. The influence of source lithologic heterogeneity on U-series disequilibrium is thus potentially important and warrants closer consideration.

Forward models for U-series isotopes in basalts that aim to investigate the likelihood of lithologic variability in the melting regime must draw on additional constraints from the mineralogy, U and Th mineral/melt partitioning, solidus depths, melting intervals, and melt productivities of mafic source lithologies (Elkins et al., 2011, 2014, 2016; Koornneef et al., 2012; Prytulak et al., 2014; Prytulak and Elliott, 2009; Russo et al., 2009; Waters et al., 2011). These models appear notably sensitive to the effects of enhanced pyroxenite melting rates, particularly when shorter lived isotopes like ^{231}Pa and ^{226}Ra are considered. Although ^{238}U-^{230}Th disequilibria are sensitive to the garnet mode of relatively garnet-rich mafic mantle lithologies, alone they can be ambiguous when trying to distinguish deep melting of garnet lherzolite from the melting of garnet pyroxenite rocks, which can occur across a broad range of mantle depths (Kogiso et al., 2004a; Lambart et al., 2013). This limitation makes the combination of ^{230}Th-^{226}Ra or ^{235}U-^{231}Pa disequilibria with ^{238}U-^{230}Th disequilibria a useful approach for identifying pyroxenite melting. In fact, high (^{230}Th/^{238}U) combined with low (^{226}Ra/^{230}Th) could be explained either 1) by melting in the presence of garnet (or perhaps high pressure aluminous clinopyroxene) followed by rapid channelized transport (e.g., Stracke et al., 2006); 2) by shallow peridotite melting within a RPF or two-porosity melting regime (Sims et al., 2002); or 3) by rapid melting of a garnet-bearing but relatively shallow lithology, such as a pyroxenite (e.g., Elkins et al., 2016). The latter scenario is illustrated in Fig. 2. Similar patterns of high (^{230}Th/^{238}U) and low, age-constrained(^{231}Pa/^{235}U) in some MORB appear even more difficult to explain without rapid melting of pyroxenite rocks: the longer half-life of ^{231}Pa allows isotopic disequilibria produced during melting to be better preserved during transport than ^{226}Ra excesses (Fig. 3c), and forward modeling calculations suggest that high melting rates due to enhanced upwelling of peridotite are insufficient to explain the particularly low ^{231}Pa excesses observed in some young basalts. The rapid melting rates of garnet-bearing pyroxenites are potentially capable of generating these patterns of disequilibria (e.g., Elkins et al., 2011; Turner et al., 2015). To explore these patterns further, below we summarize the observations of U-series isotopes in oceanic basalts to-date, and offer an updated synthesis and interpretation for their origins, including updated melt modeling techniques for U-series disequilibria that consider lithologic heterogeneity in the melt source.

4. Uranium-series isotopes in oceanic basalts

Most of the U-series disequilibrium research into oceanic basalts has incorporated some of the considerations described above and used approaches designed to investigate poorly constrained questions about basalt generation by partial melting, extraction, mixing, and transport in the mantle. In particular, many studies since the early 2000s have focused on more accurately predicting the U-series isotope compositions of basalts produced by time-dependent partial melting, using updated constraints on mineral/melt partitioning, melt productivity, melt transport and extraction timing, and melt mixing processes (e.g., Bourdon et al., 2006; Elkins et al., 2014; Prytulak et al., 2014; Russo et al., 2009; Sims et al., 2008; Stracke et al., 2006; Turner et al., 2015; Waters et al., 2011). That research has also occasionally addressed source

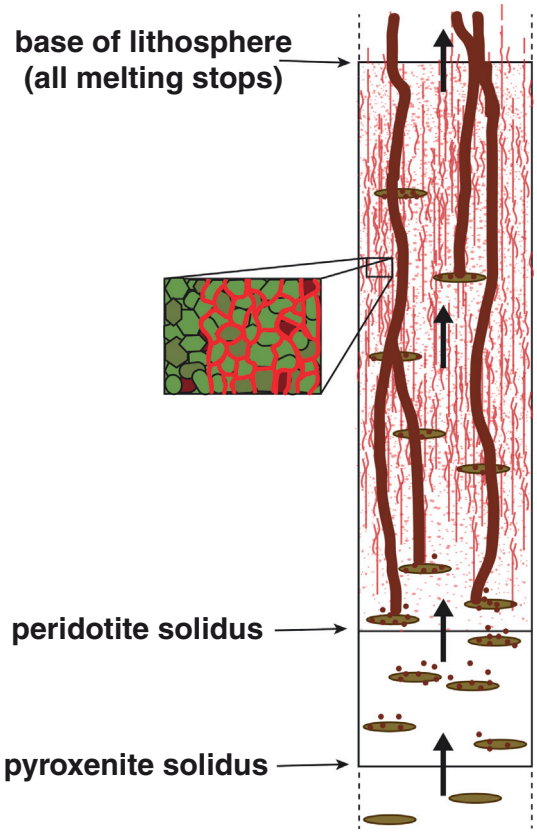

Fig. 2. Conceptual illustration for a two-lithology, two-porosity melting regime, showing an upwelling mantle column containing zones of fertile pyroxenite rock (brown ellipses) with a deeper onset of melting than ambient peridotite. Pyroxenite melting is initially shown with dark melt droplets, followed by the initiation of channels by reactive infiltration instabilities rooted in pyroxenite zones. Ambient peridotite rocks begin melting upon crossing the shallower peridotite solidus, with small melt fractions shown as pale droplets which coalesce to travel by porous flow along grain boundaries. While some peridotite partial melt may enter the larger melt channels and thereby be transported more rapidly via disequilibrium flow, the fraction that does so is unconstrained in this scenario.

heterogeneity directly. With the summary below, we primarily aim to explore the following questions: 1) What is the value of U-series isotope disequilibria with respect to understanding the role of pyroxenite in basalt generation? and 2) What do we know about magma transport with regards to pyroxenite melting in the mantle?

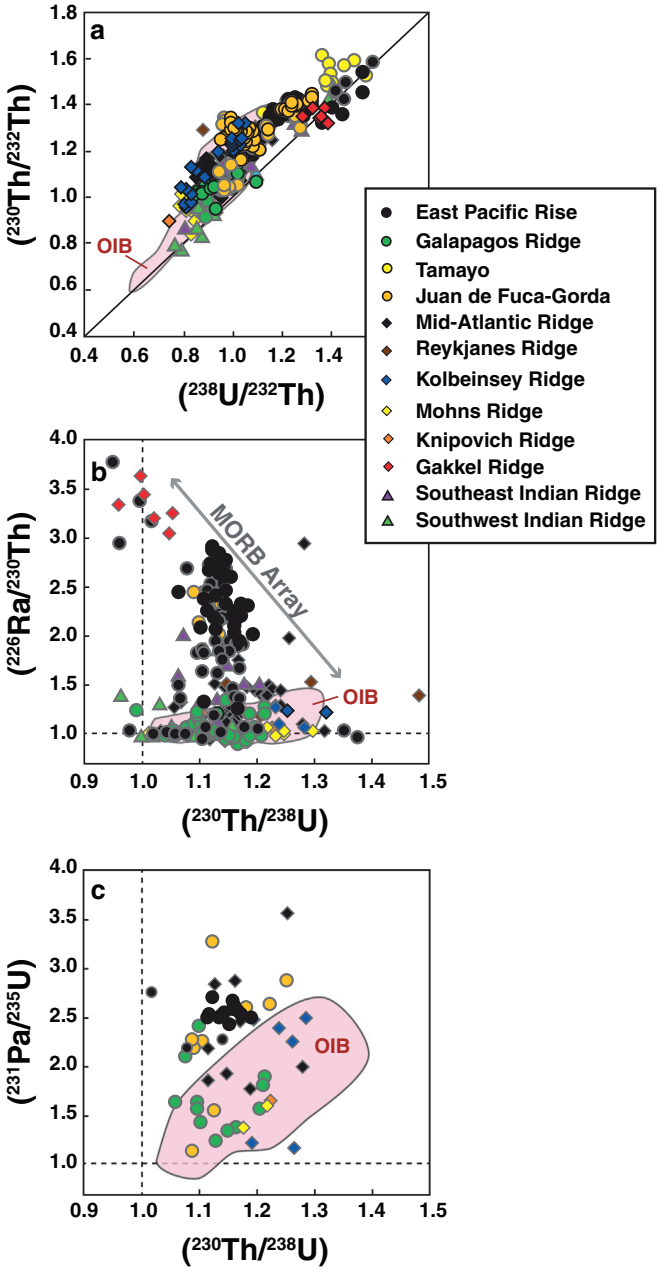

Fig. 3. a. (^{230}Th/^{232}Th) vs. (^{238}U/^{232}Th) "equiline" diagram after Allègre (1968); b. (^{226}Ra/^{230}Th) vs. (^{230}Th/^{238}U) diagram; and c. (^{231}Pa/^{235}U) vs. (^{230}Th/^{238}U) diagram showing global MORB mass spectrometry data (Bourdon et al., 1996a, 2000; Cooper et al., 2003; Elkins et al., 2011, 2014, 2016; Goldstein et al., 1989, 1992, 1993; Kokfelt et al., 2003; Lundstrom et al., 1995, 1998a, 1999; Peate et al., 2001; Reagan et al., 2017; Rubin et al., 2005; Russo et al., 2009; Sims et al., 2002; Standish and Sims, 2010; Tepley et al., 2004; Turner et al., 2015, 2016; Waters et al., 2011, 2013). In the equiline diagram, (^{238}U/^{232}Th) is proportional to U/Th elemental ratios, and systems in secular equilibrium have (^{230}Th/^{238}U) = 1.0, placing them on the equiline. All data have been filtered to omit samples with evidence for significant alteration due to interaction with seawater or seawater-derived materials, based on (^{234}U/^{238}U) ≠ 1.00 with a filtering criterion of ± 1% (see Table S1 and Supplementary Information), and to omit those with no U isotope data constraints. Data for samples with known age constraints within one-half-life of the daughter nuclide in the pairs shown (see Table S1 and Supplementary Information) are illustrated with black outlines, while other data points that lack such constraints are outlined in gray. The measured disequilibria for data points without such age indicators are considered minimum values, as U-series disequilibria could have been reduced by age decay since eruption. Global OIB data after Fig. 4 are shown as red fields.

4.1. Mid-ocean ridge basalts

Fig. 3 shows global MORB data for U-series isotopes, compiled from the global literature and filtered for data quality and age constraints (see Table S1 and Supplementary Information). Global MORB samples mostly exhibit (^{230}Th/^{238}U) > 1.0, indicating melting occurs in the presence of garnet or high-pressure clinopyroxene with bulk rock partition coefficients of $D_U > D_{Th}$ (e.g., Blundy and Wood, 2003). In mantle melting dominated by a single lithology, (^{226}Ra/^{230}Th) is expected to be sensitive to variations in residual melt porosity (e.g., Sims et al., 1999), as well as aging after melt segregation, such as in magma chambers, during channelized melt transport through the mantle and lithosphere, and after eruption (Condomines et al., 2003; Cooper et al., 2003; Koornneef et al., 2012; Rubin et al., 2005; Saal and Van Orman, 2004; Sims et al., 2003, 2008), although many of the samples included here are constrained for eruption age (Figs. 3-4). (^{226}Ra/^{230}Th) and (^{230}Th/^{238}U) are broadly negatively correlated in age-constrained, unaltered global MORB, particularly for ridges away from hotspots (Fig. 1b). Basalts from hotspot-adjacent ridges, as well as specific areas with independent geochemical evidence for particularly enriched, heterogeneous mantle (e.g., Elkins et al., 2014) have lower (^{226}Ra/^{230}Th) ratios, similar to those of OIB, as addressed in greater detail below. No systematic global relationship is clearly observed between (^{231}Pa/^{235}U) and (^{230}Th/^{238}U) (Fig. 1c).

Interpretations for the negative (^{226}Ra/^{230}Th) versus (^{230}Th/^{238}U) array have focused on two-porosity flow and progressive melt depletion of a relatively homogeneous mantle source (e.g., Elkins et al., 2011; Sims et al., 2002), i.e. the ongoing evolution of melts derived from a source that is progressively depleted in incompatible elements by continuous melting over time. For example, similar to observations of Sims et al. (2002) for age-constrained basalts from 9°N EPR, Elkins et al. (2011) demonstrated that U-series isotopic compositions in MORB from the southern Kolbeinsey Ridge, with their depleted Nd isotope signatures, moderately high (^{230}Th/^{238}U), and high (^{231}Pa/^{235}U) and (^{226}Ra/^{230}Th), can be explained by garnet lherzolite melting without lithologic source heterogeneity.

However, characteristics of U-series isotopes in MORB from numerous regions (specifically, high ^{230}Th excess and low ^{226}Ra and ^{231}Pa excesses), coupled with additional geochemical evidence (e.g., enriched radiogenic isotopes, characteristic trace element ratios), more strongly favor lithological heterogeneity in the local mantle source (e.g., Rubin and Macdougall, 1992), as shown by the following examples. Lundstrom et al. (1998b) favored pyroxenite veins in the melt source to explain ^{238}U-^{230}Th and ^{235}U-^{231}Pa disequilibria in basalts from the Mid-Atlantic Ridge at 33°S, and Lundstrom et al. (1999) suggested that U-series disequilibria from the Siquieros Transform and Lamont seamounts are products of channelized flow caused by reactive infiltration during melting of heterogeneous, enriched domains. Russo et al. (2009) likewise used forward model calculations invoking a small fraction of pyroxenite veins to explain Southeast Indian Ridge basalt compositions. They tested both RPF and dynamic melting models and proposed lithological heterogeneity as the best explanation for local variations in both U-series disequilibria and axial depth (a proxy for crustal thickness and thus total magma supply to the ridge). Waters et al. (2011) conducted similar calculations to demonstrate that E-MORB from the EPR are best explained by a combination of 1) channelized transport and two-porosity flow with progressive source depletion, and 2) mixing of melts from a lithologically heterogeneous source. Dynamic melt model calculations from Turner et al. (2015) also favor lithological heterogeneity beneath the Mid-Atlantic Ridge at 5-11°S. Elkins et al. (2011, 2014, 2016) further demonstrated from both RPF and dynamic melting models that mixing of pyroxenite-derived and peridotite-derived melts is likely necessary to explain basalt compositions from specific

areas along the North Atlantic ridge system, particularly low age-constrained ($^{226}Ra/^{230}Th$) and ($^{231}Pa/^{235}U$) ratios combined with high ($^{230}Th/^{238}U$). In fact, melting of peridotite at any upwelling rate tested failed to produce sufficiently high ^{230}Th or sufficiently low ^{226}Ra and ^{231}Pa excesses to explain observations from the Northern Kolbeinsey Ridge in particular, while pyroxenite melting, thanks to their elevated melting rates, closely approached the observed data (Elkins et al., 2011, 2016).

In brief, the observations and modeling results summarized above suggest that models for U-series disequilibrium in MORB can differentiate between rapid melting due to fast upwelling and melting of more fusible mafic lithologies. As explored above, we broadly expect both that partial melting of a second, more fertile lithology generates high-porosity channels, and that the geochemical signatures of such pyroxenite melts are preserved during disequilibrium (fractional or near-fractional) transport along channels (e.g., Faul, 2001; Weatherley and Katz, 2012, 2016) (Fig. 2). However, two-porosity and reactive infiltration instability models have indicated that in the presence of melt channels, some magma is simultaneously transported via reactive flow in adjacent low-porosity zones (Jull et al., 2002), and that such melts may not segregate efficiently into adjacent channels due to cold sheath effects (Weatherley and Katz, 2016). As a result, while some of the peridotite partial melt in a two-lithology region beneath mid-ocean ridges may enter rapid transport channels, effectively experiencing dynamic melting, we can reasonably expect a detectable portion of the peridotite melt to experience an RPF process instead, much like the single-lithology, two-porosity flow suggested for MORB in more homogeneous settings (Sims et al., 2002; Waters et al., 2011).

4.2. Ocean island basalts and hotspot-ridge interaction settings

Broadly, the study of ocean island magmatism attempts to investigate the presence and characteristics of deep-seated mantle plumes as the principal drivers of global intraplate hotspot volcanism, and to better understand the origin and role of long-term geochemical heterogeneity in the mantle. The well-documented geochemical variations observed in global OIB suggest that hotspot partial melting regimes might sample a more diverse mantle source than divergent boundaries. However, the lithologic makeup of the global OIB source mantle is also widely debated. Uranium-series disequilibria offer a useful additional method for further investigating the question of lithologic heterogeneity in mantle plumes and the source regions for hotspot volcanism.

Uranium-series isotope measurements from ridge settings adjacent to hotspots are included in Fig. 3, and global U-series isotopic data for OIB are shown in Fig. 4. Overall, OIB and hotspot-adjacent ridge basalts have lower ^{226}Ra and ^{231}Pa excesses than MORB, along with relatively high ($^{230}Th/^{238}U$) and lower (i.e., more enriched) U/Th ratios (expressed as ($^{238}U/^{232}Th$)) (Figs. 3a, 4a; Table S1). These patterns generally favor high melting rates in the presence of residual garnet (e.g., Bourdon et al., 1998, 2006; Pickett and Murrell, 1997; Sims et al., 1999). These isotopic compositions may mainly reflect elevated mantle potential temperatures, causing a higher proportion of melting to occur in the garnet peridotite stability field (e.g., Bourdon et al., 1996b), and the enhanced, "active" upwelling of a mantle plume (i.e., solid upwelling rates on the order of meters per year; Hauri et al., 1994a; Kelemen et al., 1997); alternatively, they could indicate a higher abundance of highly fusible garnet pyroxenite in the melt zone (e.g., Hirschmann and Stolper, 1996). Deconvolving these two effects is particularly important when interpreting OIB data to explore the petrogenetic and geodynamical questions described above. Both processes are likely involved in OIB genesis but, in some cases, the U-series disequilibria may be dominated by one of the two processes (e.g., Bourdon et al., 1998, 2005; Elkins et al., 2016; Prytulak and Elliott, 2009; Sims et al., 1999, 2008; Turner et al., 1997). Moreover, to meaningfully investigate mantle lithologies involved during partial melting at ocean island settings, modeling of partial melting must also incorporate a number of additional factors specific to this geologic setting. Mid-ocean ridge settings are envisioned using two-dimensional, triangular mixing regimes (e.g., Langmuir et al., 1992), with thin to nonexistent lithosphere and oceanic crustal thicknesses up to ~6–7 km (e.g., Bown and White, 1994). In contrast, modeling of partial melting beneath ocean islands is typically addressed using one-dimentional melting columns, and assuming that OIB typically erupt through thickened seafloor crust overlying comparatively thick mantle lithosphere that effectively truncates the mantle melting regime (e.g., Bourdon and Sims, 2003; Niu et al., 2011; Olson, 1988; Ribe, 1988; Sims and Hart, 2006). Due to their mostly subaerial exposures and historical records, many ocean island basalts are age-constrained by historic data and stratigraphy, making

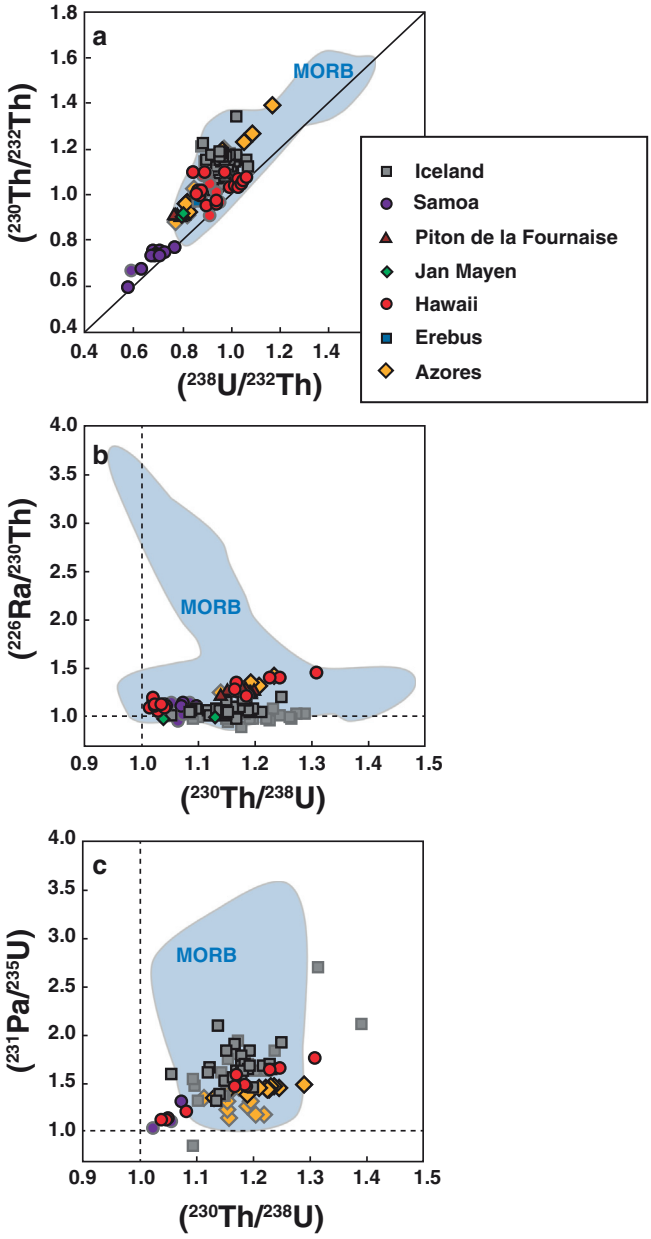

Fig. 4. a. ($^{230}Th/^{232}Th$) vs. ($^{238}U/^{232}Th$) "equiline" diagram; b. ($^{226}Ra/^{230}Th$) vs. ($^{230}Th/^{238}U$) diagram; and c. ($^{231}Pa/^{235}U$) vs. ($^{230}Th/^{238}U$) diagram showing global ocean island basalt mass spectrometry data (Cohen and O'Nions, 1993; Elkins et al., 2016; Kokfelt et al., 2003; Koornneef et al., 2012; Peate et al., 2001; Pietruszka et al., 2001, 2009; Prytulak et al., 2014; Prytulak and Elliott, 2009; Reagan et al., 2017; Rubin et al., 2005; Sims et al., 1995, 1999, 2008; Sims and Hart, 2006; Stracke et al., 2003c, 2006; Turner et al., 2016) (see Table S1 and Supplementary Information). Global MORB data from Fig. 3 are shown as blue fields. Filtering criteria and age constraints are as in Fig. 3.

initial ^{230}Th-^{226}Ra and ^{235}U-^{231}Pa disequilibria at eruption well-characterized (see Fig. 4, and references therein). However, passing through thicker crust and lithosphere can result in greater degrees of crustal assimilation, as observed at certain Azores islands, Reunion, Iceland, and the Canaries (Bourdon et al., 1998; Claude-Ivanaj et al., 1998; Koornneef et al., 2012; Lundstrom, 2003; Pietruszka et al., 2009; Prytulak et al., 2014; Turner et al., 2017).

Taking the above considerations into account, U-series disequilibrium studies of OIB have provided extensive evidence for mantle upwelling rate variations at ocean island settings, with or without involvement of a second lithology. Where expected upwelling rates and melting rates are particularly high, such as Hawaii, residence times of U-series nuclides in the melting column are low, and thus ingrowth is limited and melting can approach time-independent melting outcomes (Elliott, 1997; Sims et al., 1995, 1999). In locations with slower upwelling, the effects of daughter nuclide ingrowth during melting become more significant. Bourdon et al. (2006) calculated U-series disequilibria in partial melts using solid mantle upwelling rates predicted from the estimated buoyancy fluxes for a range of global hotspots, and compared their results with (^{230}Th/^{238}U) and (^{231}Pa/^{235}U) observed in OIB. They observed global negative correlations between measured (^{230}Th/^{238}U) or (^{231}Pa/^{235}U) ratios and buoyancy fluxes at ocean islands. Based on their modeling results, they suggested that both upwelling velocity and mantle potential temperature at hotspots influences U-series disequilibria in partial melts, in support of a mantle plume origin for ocean island settings. However, they did not call for source lithologic heterogeneity to explain their global observations. Likewise, in the Azores, both enhanced upwelling and compositional heterogeneity have been suggested as factors involved in basalt generation, but studies have overall not supported pyroxenite rocks as the primary hosts for that heterogeneity, instead suggesting either hybridized/refertilized peridotites or a water-rich source (Bourdon et al., 2005; Claude-Ivanaj et al., 2001; Prytulak et al., 2014; Prytulak and Elliott, 2009; Turner et al., 1997).

It is important to be able to distinguish upwelling variations from the enhanced melting rate effects of a highly fusible source beneath oceanic hotspots. Contradictory interpretations of the lithologic nature of the Hawaiian mantle help to illustrate the difficulties in this task: Sims et al. (1999) observed a positive correlation between (^{231}Pa/^{235}U) and (^{230}Th/^{238}U) in Hawaiian lavas, which they modeled using both dynamic and RPF models and interpreted to reflect decreasing upwelling rates with increasing distance from the center of the hotspot. Stracke et al. (1999) further suggested that the contribution of pyroxenite melting could not explain the correlations between ^{238}U-^{230}Th disequilibria and radiogenic isotopes in Hawaiian basalts. Additionally, Phillips et al. (2016) measured U-series disequilibria in basanites from Haleakala at the trailing end of the Hawaiian hotspot, and suggested that the heterogeneous mantle source they observed was best explained by non-pyroxenite heterogeneities. Stracke et al. (1999)'s modeling, however, tested whether Hawaiian basalts are representative of a single magmatic series, with magma mixing along a single melting column. The observed correlations between ^{238}U-^{230}Th disequilibria and radiogenic isotopes could alternatively be explained by spatial variations in the plume source: Mauna Loa is centered on the plume and, hence, overlies a zone with a higher mantle potential temperature than Haleakala, leading to higher mantle buoyancy and potentially allowing a larger proportion of pyroxenite in the source (Sobolev et al., 2005) and a higher melting degree for both peridotite and pyroxenite. The mantle source of Haleakala could contain a much smaller quantity of such lithological heterogeneities. This alternative explanation is supported by Pietruszka et al. (2001), who measured ^{238}U-^{230}Th-^{226}Ra disequilibria in historic samples from Kilauea, and found a better fit to low (^{226}Ra/^{230}Th) ratios and small variations over time by modeling the effects of melting a lithologically heterogeneous source with both dynamic and RPF model calculations. Hence, we suggest that variations in U-series disequilibria in Hawaiian basalts and overall magma production cannot be explained solely by the contribution of pyroxenite rocks to a single melting regime, but that radial distribution of both mantle potential temperatures and the amount of pyroxenite in the source can impact localized magma generation over time.

Variations in U-series disequilibria due to changes in upwelling rate have been observed in other locations, similarly indicating a radial distribution in upwelling rates and thereby offering additional support for mantle plume models: Kokfelt et al. (2005) suggested that mantle upwelling is greater towards the plume center in the Galapagos, and various studies of U-series isotopes in Icelandic basalts have also called for faster upwelling near the hotspot center (Kokfelt et al., 2003; Koornneef et al., 2012; Peate et al., 2001; Sigmarsson and Steinthórsson, 2007; Stracke et al., 2003b, 2003c; Stracke and Bourdon, 2009; Turner et al., 2016). Again, in these studies, lithological heterogeneity was further invoked to explain the compositional data. While Kokfelt et al. (2005) did not specifically test for a pyroxenite source, studies focused on Icelandic basalts have explicitly considered two-lithology pyroxenite and peridotite melting variations. Finally, additional geochemical evidence, such as trace element enrichment and radiogenic isotopic signatures, coupled with U-series disequilibria, has more explicitly supported the presence of lithological heterogeneity in the mantle source (e.g., Elkins et al., 2016; Gurenko et al., 2009; Koornneef et al., 2012; Lundstrom et al., 2003; Sigmarsson et al., 1998).

As discussed above, U-series disequilibria have been instrumental for exploring both enhanced upwelling and source heterogeneity in generating OIB, but suggested explanations for the precise nature of that heterogeneity (e.g., refertilized peridotite, MORB-like eclogite, olivine-bearing pyroxenite, amphibole-bearing veins) have varied. This range in proposed scenarios is partly the product of changes or improvements in constraints on pyroxenite and peridotite melting and in melt modeling methods over time (for example, the measurement of more appropriate partition coefficients for mafic lithologies; e.g., Elkins et al., 2008; Pertermann and Hirschmann, 2003b; Pertermann et al., 2004), as well as simply the range of modeling choices available and potential for non-unique results. In essence, some hotspots may overlie mantle plumes that entrain a higher proportion or more fertile composition of pyroxenite rocks than others; and in some plumes, disparate lithologies may become more efficiently homogenized or mixed by hybridization processes than in others. Uranium-series isotope studies, as a method, have overall been successful at identifying these variations, though they are most effective when combined with trace element and radiogenic isotope data to fully explore the nature of a particular hotspot and its heterogeneous origins, and when the choice of melt models used is thoughtful and well-informed. On the whole, it appears that lithologic heterogeneity does play a role in the origin of many hotspots. Furthermore, both rapid melting rates, and the need to extract melts from a regime hosting a high degree of heterogeneity, may more strongly favor dynamic, channelized melt transport over porous flow scenarios for hotspots.

4.3. Outstanding questions

Uranium-series isotopic disequilibria in oceanic basalts are produced by factors that vary on a global scale: upwelling rates, mixing efficiency, transport regimes, mantle temperature, and the amount and nature of heterogeneities. The relative importance and nature of pyroxenitic lithologies in the global mantle melt regime remains uncertain, and methods to test for pyroxenitic melting can be complex and insufficiently constrained. Nonetheless, decades of research have produced genuine constraints, and there is potential to better answer questions about oceanic basalt production by better aligning modeling methods with current interdisciplinary understanding. Uranium-series disequilibria in young, unaltered basalts are thus a promising tool in the geochemical arsenal for investigating and detecting mantle heterogeneity.

In a few cases, the interpretation of U-series disequilibria has beneficially drawn from thermodynamic models and melt parameterizations produced by the geochemical and petrologic communities, such as

pMELTS (Ghiorso et al., 2002). While limited by the uncertainties in partition coefficient measurements, more appropriate measurements now exist for a range of pyroxenite mineral compositions than were available 20 years ago (e.g., Elkins et al., 2008; Pertermann et al., 2004; Pertermann and Hirschmann, 2003b; Spandler et al., 2017). Published methods for continuous numerical solutions also exist for both dynamic and RPF model scenarios (Bourdon et al., 2005; Spiegelman, 2000; Zou and Zindler, 2000). To demonstrate one useful approach, below we test new forward modeling calculations of U-series isotopes during partial melting of a bi-lithologic mantle, and compare our results to the global oceanic basalt U-series data set (Figs. 3-4; Table S1). Our primary goals with the models selected are 1) to suggest a family of modeling methods that the geochemistry community can access for future research, and 2) to produce initial melt modeling results that both synthesize and build on the U-series disequilibrium modeling efforts of recent decades.

A number of outstanding questions about oceanic basalt petrogenesis are directly relevant to the subject of mantle lithologic composition, and we target and explore some of them below. For instance, to what extent is partial melting of pyroxenite necessary to explain oceanic basalt compositions? How are basaltic partial melts likely transported through the mantle, and how much is that transport style related to source heterogeneity? How much do changes in melt productivity and partitioning behavior during the melt process affect basalt compositions?

5. Uranium-series as a tool for detecting mantle heterogeneity

5.1. Melting model rationale

Time-dependent forward modeling of the U-series disequilibria produced during partial melting is the main technique used to interpret measured disequilibria in oceanic basalts, but the method has known limitations. It is necessary to be aware of these limitations prior to interpreting melt modeling results. Sims et al. (1999, 2002), Pietruszka et al. (2001), Bourdon and Sims (2003), Prytulak et al. (2014), Williams and Gill (1989) and Elkins et al. (2011), among others, documented the particularly high degree to which model outcomes are sensitive to very small changes in bulk U and Th partition coefficients – changes significantly smaller than the uncertainties involved in the measurement and calculation of both mineral/melt partition coefficients and hypothesized bulk rock mineral modes (Lundstrom et al., 2000). Moreover, partition coefficients for U and Th in mantle minerals significantly depend on mineral composition (e.g., Elkins et al., 2008). Thus, a poor choice of values used in a model calculation could be both inappropriate and highly consequential for model outcomes (e.g., Elkins et al., 2011). For example, the use of clinopyroxene and garnet U and Th partition coefficients from peridotite melting experiments to calculate bulk rock partition coefficients for a typical MORB-like eclogite can result in erroneous predictions for ($^{230}Th/^{238}U$) in basaltic partial melts (e.g., Stracke et al. (1999) versus Elkins et al. (2016)). Where possible, we thus have limited our choices of partition coefficients (Table 1) to sources with the following experimental characteristics: 1) researchers used similar starting material compositions to our lithology of interest (i.e., fertile peridotite, eclogite, or olivine-bearing pyroxenite); 2) measurements were made for experiments that reached equilibrium at an appropriate pressure to simulate mantle melting conditions; 3) wherever possible, experimental runs were chosen where multi-phase solids grew together (e.g., clinopyroxene and garnet that crystallized together in equilibrium, rather than selecting clinopyroxene values from one experiment and garnet from another); and 4) researchers conducted experiments using assemblages that limited the range of oxygen fugacity conditions, such as a graphite capsule. One-atmosphere experiments of crystallizing basaltic liquids were thus avoided, as were conditions that may have increased the oxidation state of U and thus reduced the mineral/melt partition coefficients of U. In a few cases, exceptions were made for partitioning behavior in spinel and plagioclase due to a relative dearth of experimental measurements (see Table 1 for further details).

Both dynamic and RPF modeling techniques also require additional input parameters that can result in a range of non-unique solutions (e.g., solidus depths, permeability variations, upwelling rates, matrix porosity, etc.). Between these sources of uncertainty in model output and interpretation – and not even considering issues like melt productivity estimates or the amount and type(s) of pyroxenite in the source regions (e.g., Hauri et al., 1994b) – it is unwise to use such melting models to attempt to quantitatively match precise maximum residual melt porosities or solid mantle upwelling rates to measured basalt compositions without drawing on additional information or using comparative approaches. However, with additional evidence such as radiogenic isotope compositions, buoyancy flux estimates of mantle upwelling rates at hotspots, and geochemical indicators of local mantle temperature, greater accuracy may be possible (e.g., Fig. S2). We thus encourage

Table 1
Fixed mineral/melt partition coefficients used to calculate bulk rock partition coefficients in model calculations for this study.

Lithology	Phase	D_U	D_{Th}	D_{Pa}[a]	D_{Ra}[a]	Source
Garnet peridotite	Garnet	0.038	0.017	0.00001	0.00001	RD 1097-5 experiment, Salters et al. (2002)
	Clinopyroxene	0.003	0.004	0.00001	0.00001	RD 1097-5 experiment, Salters et al. (2002)
	Olivine	0.00005	0.00047	0.00001	0.00001	RD 1097-5 experiment, Salters et al. (2002)
	Orthopyroxene	0.0078	0.0086	0.00001	0.00001	TM0500-3 experiment, Salters et al. (2002)
	Spinel	0.012	0.0024	0.00001	0.00001	Lunar basalt, Klemme et al. (2006)
Spinel peridotite	Clinopyroxene	0.008	0.007	0.00001	0.00001	TM 1094-9 experiment, Salters and Longhi (1999)
	Olivine	0.00005	0.00047	0.00001	0.00001	RD 1097-5 experiment, Salters et al. (2002)
	Orthopyroxene	0.0024	0.0027	0.00001	0.00001	RD 1097-2 experiment, Salters et al. (2002)
	Plagioclase	0.0006	0.0034	0.00001	0.02000	D_U, D_{Th} calculated after Blundy and Wood (2003); D_{Ra} from Fabbrizio et al. (2009)
	Spinel	0.012	0.0024	0.00001	0.00001	Lunar basalt, Klemme et al. (2006)
Gb-108 pyroxenite [b]	Garnet	0.02405	0.00415	0.00001	0.00001	A343 experiment, Pertermann et al. (2004)
	Clinopyroxene	0.0041	0.0032	0.00001	0.00001	A343 experiment, Pertermann et al. (2004)
	Olivine	0.00005	0.00047	0.00001	0.00001	RD 1097-5 experiment, Salters et al. (2002)
	Plagioclase	0.0006	0.0034	0.00001	0.02000	D_U, D_{Th} calculated after Blundy and Wood (2003); D_{Ra} from Fabbrizio et al. (2009)
	Spinel	0.046	0.016	0.00001	0.00001	Maximum measured, Elkins et al. (2008)
MIX1G pyroxenite	Garnet	0.013	0.0032	0.00001	0.00001	Experimental results, Elkins et al. (2008)
	Clinopyroxene	0.017	0.015	0.00001	0.00001	Experimental results, Elkins et al. (2008)
	Olivine	0.00005	0.00047	0.00001	0.00001	RD 1097-5 experiment, Salters et al. (2002)
	Spinel	0.046	0.016	0.00001	0.00001	Maximum measured, Elkins et al. (2008)
	Orthopyroxene	0.0078	0.0086	0.00001	0.00001	TM0500-3 experiment, Salters et al. (2002)
	Plagioclase	0.0006	0.0034	0.00001	0.02000	D_U, D_{Th} calculated after Blundy and Wood (2003); D_{Ra} from Fabbrizio et al. (2009)

[a] By convention, D_{Pa} and D_{Ra} are set equal to very small values (1×10^{-5}) for most minerals, except D_{Ra} in plagioclase.
[b] There are no appropriate published partitioning data for U, Th, Ra, or Pa in quartz, kyanite, or coesite, and the mineral/melt partition coefficients in these minerals are expected to be extremely low. To simplify the calculations in this paper, the D_i values for these three minerals are assumed to be zero.

a comprehensive approach to analytical studies of U-series in oceanic basalts, incorporating a complete geochemical data set wherever possible and thoughtfully choosing appropriate melt modeling methods.

Below, we aim to prioritize key advancements in forward modeling of U-series disequilibria during partial melting. Recent calculations for two-lithology melting scenarios have incorporated thermodynamic predictions from models such as pMELTS (Ghiorso et al., 2002), but for the most part, this has not been fully integrated with past U-series disequilibrium calculations and we add that effort here. Previous U-series work has also used models that consider variable partition coefficients, but typically not variable productivities for each lithology during melting (e.g., Stracke et al., 2003b, 2003c; Stracke and Bourdon, 2009). We note that such productivity variations are likely important for both peridotite and pyroxenite lithologies (e.g., Asimow et al., 2001; Hirschmann and Stolper, 1996; Pertermann and Hirschmann, 2003a). While numerical solutions for U-series disequilibria in RPF melting models have been used previously to consider variable productivities during melting (Elkins et al., 2011, 2014, 2016; Koornneef et al., 2012; Russo et al., 2009; Waters et al., 2011), the constraints available at the time for pyroxenite and two-lithology melt productivity were limited. Numerical solutions for U-series isotopes in dynamic melting have also permitted consideration of variable productivities, but again, with limited constraints at the time, and using fixed bulk partition coefficients throughout the melting column (Bourdon et al., 2005).

Here we integrate calculated information gathered from pMELTS (Ghiorso et al., 2002), Melt-PX (Lambart et al., 2016), thermal exchange models for two-lithology melting (Lambart, 2017), and continuous one-dimensional numerical solutions for both RPF and dynamic melting that permit both bulk partition coefficients and melt productivities to vary non-linearly (after Bourdon et al., 2005; Spiegelman, 2000). To limit our effort to an initial demonstration and test of the method, we avoid calculating the effects of factors that are poorly constrained and far more complex (such as the dependence of mineral/melt partition coefficients on residual mineral compositions, two-porosity melting regimes, and the role of reactive infiltration instabilities in generating and preserving channelized flow). However, our models capture many of the major factors expected to influence U-series during partial melting, i.e. variations in trace element partitioning, transport mechanisms, and time scales of melting. We further note that the inclusion of both RPF and dynamic melting models effectively presents both "end member" melt transport scenarios envisioned by two-porosity models, though we do not assess magma mixing in such an environment, as this topic has been extensively addressed elsewhere (e.g., Jull et al., 2002; Weatherley and Katz, 2012). In the interest of limiting the scenarios used here to simpler initial test conditions, we also have omitted more complex mixing and summing schemes (such as triangular melt regimes for mid-ocean ridge settings after Langmuir et al. (1992) or statistical mixing models after Rudge et al. (2013)), as well as volatile effects on melting, a range of different lithospheric thicknesses that truncate melt columns, decay during time elapsed while segregated dynamic partial melts travel along melt channels, and scenarios with different quantities of pyroxenite in the melt source. We consider all of these scenarios to be interesting potential future directions for further study.

5.2. Implications for marine basalt generation from a lithologically heterogeneous source

5.2.1. Melt-PX calculations

To calculate the melt fraction and the mineral modes along the melting column, we followed an approach similar to Lambart (2017) to test several scenarios of broad relevance to MORB and OIB generation. We first used the Melt-PX calculator (Lambart et al., 2016) to model the decompression melting of a two component (pyroxenite and peridotite) mantle containing 10% pyroxenite and 90% peridotite rocks. Results from the Melt-PX calculations included the temperatures *(T)* and predicted melt fractions *(F)* for both pyroxenite and peridotite rocks as a function of pressure *(P)* (see Table S2). After Lambart (2017), we

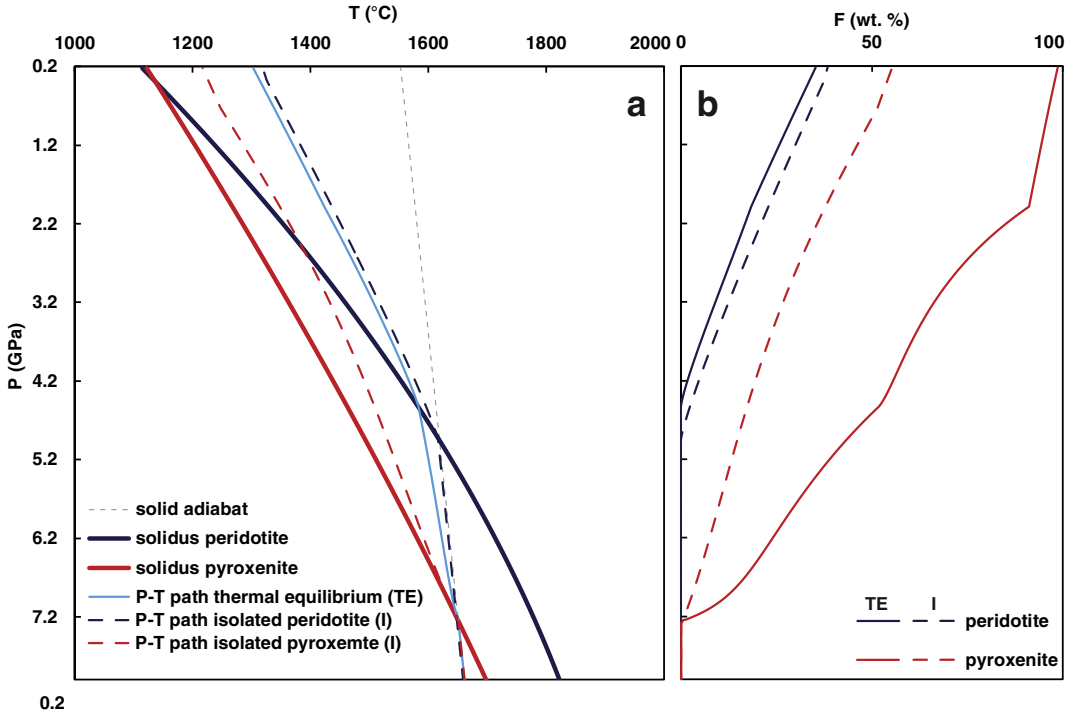

Fig. 5. a. Pressure (*P*) - Temperature (*T*) diagram illustrating one set of model calculations from Melt-PX, showing solidus conditions and adiabatic melting paths for peridotite and coexisting Gb-108 pyroxenite under thermal equilibrium (TE) and thermally isolated (I) conditions at $T_p = 1550$°C. b. Pressure (*P*) - melt fraction (*F*) diagram for the same set of calculations, illustrating the effects of thermal isolation versus equilibration on melt productivity.

considered two cases: (1) the two lithologies are in thermal equilibrium but chemically isolated, and (2) the two lithologies are isolated both chemically and thermally (Fig. 5), to determine whether thermal equilibration has a notable effect on U-series isotope outcomes during partial melting, as it does for trace element models (Lambart, 2017). Calculations were performed for two different pyroxenite compositions (MIX1G and Gb-108) and at two different mantle potential temperatures (T_p = 1300 and 1550 °C). MIX1G is a silica-deficient pyroxenite with a composition close to the average of natural pyroxenites referenced in the literature (Hirschmann et al., 2003), while Gb-108 is a silica-excess pyroxenite with the composition of a natural olivine gabbro (Yaxley and Sobolev, 2007). The peridotite composition used here and for the subsequent pMELTS calculations (see below) matches the depleted "DM" composition from Salters and Stracke (2004). Initial clinopyroxene modes for the peridotite were determined for the DM composition using the fraction of clinopyroxene predicted by pMELTS (Ghiorso et al., 2002) at the pressure that the peridotite crosses its solidus (i.e., 20 wt.% at ~4.5 GPa for T_p = 1550°C and 18 wt.% at 1.8 GPa for T_p = 1300°C) (Table S2).

5.2.2. pMELTS approach

Following the Melt-PX calculations, we used pMELTS (Ghiorso et al., 2002) with the alphaMELTS front-end (Smith and Asimow, 2005) to calculate equilibrium residual phase assemblages along the adiabatic decompression paths determined from Melt-PX. For each *P-F* condition, we calculated the residual mineral phase assemblage using isobaric batch melting only; Lambart (2017) previously showed that the chosen pMELTS melting regime (continuous, fractional, or batch) does not significantly affect the phase assemblage, and consequently will not significantly affect the bulk partition coefficients for each pressure increment. For each lithologic component, an initial pMELTS run was performed using the pressure calculated with Melt-PX where F = 0.5%. Subsequent runs were performed at pressure steps of 0.01 GPa. In each pMELTS run, we used the following approach: (1) calculations were made at fO_2 = FMQ − 1 (i.e. the fayalite-magnetite-quartz buffer minus one log unit); (2) Cr_2O_3 and MnO were omitted from the calculations, because pMELTS is not calibrated for MnO and Cr_2O_3 in solid phases, leading to erroneous results for these elements (these elements were not included in the pyroxene and garnet calibrations for pMELTS) (Asimow et al., 1995); and (3) we used the old garnet calibration model. This choice was made because in the absence of chromium, the new garnet model strongly overestimates the stability range for garnet (see Fig. 1 in Lambart et al., 2016).

Bulk partition coefficients for each lithology were then calculated using the residual mineral modes at each pressure step determined using pMELTS (Fig. 6), with the fixed mineral/melt partition coefficients shown in Table 1 for each lithologic type. Due to the overall lack of constraints on the effects of mineral composition on mineral/melt partition coefficients for the minerals and elements in question, we did not attempt to calculate partition coefficient values using mineral compositions here. We note that this can potentially create a discontinuous change in bulk rock partition coefficients for peridotite lithologies at garnet-out, not only because garnet is absent but because clinopyroxene partition coefficient values change at the transition. This effect neglects the possibility of more gradual changes to the bulk partition coefficients due to changes in clinopyroxene composition leading up to the moment garnet disappears from the assemblage. Until more robust compositional constraints are available for calculating the U and Th partition coefficients of clinopyroxene based on mineral composition, however, we consider this approach the best available option.

5.2.3. Dynamic melting calculations of ^{238}U-^{230}Th-^{226}Ra and ^{235}U-^{231}Pa disequilibria

The dynamic melting calculations are based on the equations of McKenzie (1985) that were later modified by Richardson and McKenzie (1994) to include non-modal melting and variable partition coefficients (their equations 10 and 11). We numerically integrated these equations using the MATLAB software and performed

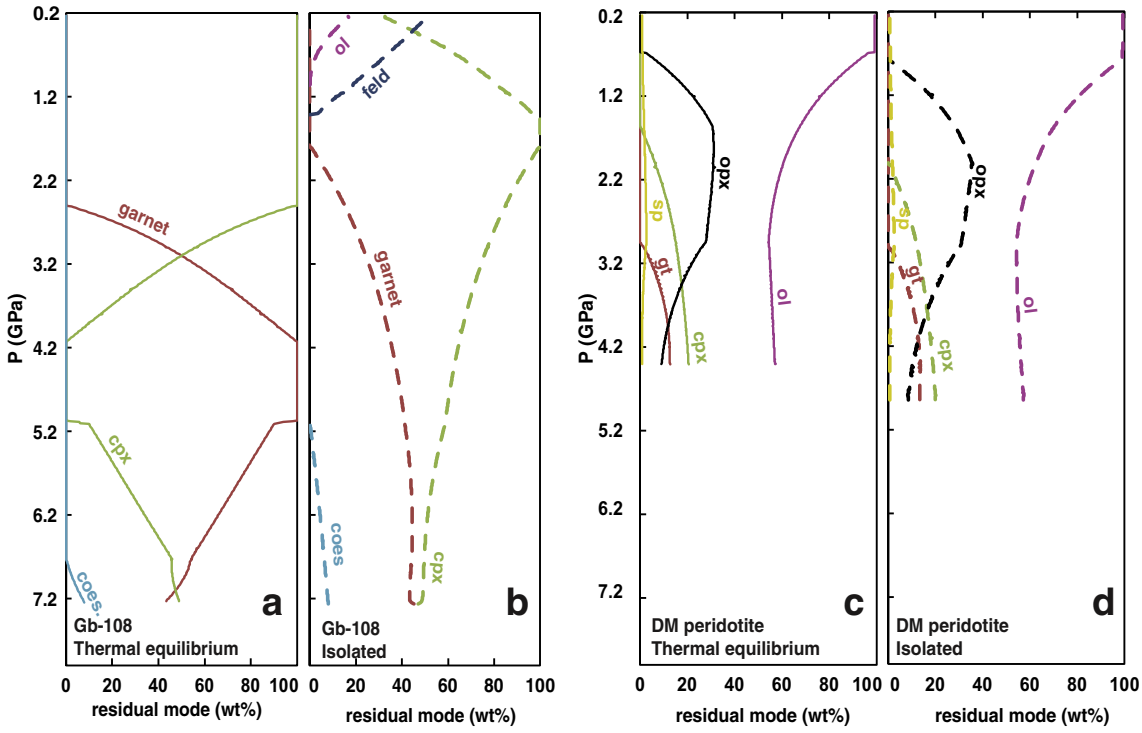

Fig. 6. Modes of minerals present with depth during melting for the calculations shown in Fig. 5. Modes, calculated with pMELTS at given *P-F* conditions, are shown for a. Gb-108 in thermal equilibrium, b. Gb-108 in thermal isolation, c. peridotite in thermal equilibrium, and d. peridotite in thermal isolation (coes: coesite, cpx: clinopyroxene, feld: feldspar, gt: garent, ol: olivine, opx: orthopyroxene, sp: spinel).

calculations for constant solid upwelling rates and melt porosity values along a one-dimensional melt column. The initial conditions for integration corresponded to a batch melt with a degree of melting equal to the matrix porosity, and the equations were integrated up to a depth corresponding to the base of the lithosphere. The bulk partition coefficients and degree of melting (and hence the melting rate) as a function of depth and pressure were drawn from the results of the calculations outlined in Sections 5.2.1 and 5.2.2.

To determine the U-series isotope disequilibria in the instantaneous partial melts, we determined a best-fit formula for the degree of melting as a function of pressure; this formula was then used to calculate the melting rate and degree of melting at each pressure step. For the peridotite scenarios, the degree of melting F was fitted using the polynomial function:

$$F = a_{per} \times P + b_{per} \quad (1)$$

where a_{per} and b_{per} are the best-fit polynomial coefficients for each peridotite melting scenario.

The melting rate (Γ) was then calculated with the following equation:

$$\Gamma = \rho_s W \frac{dF}{dz} \quad (2)$$

where W is the solid upwelling rate, z is the vertical depth coordinate, and ρ_s is the density of the solid matrix. This equation can be further modified if one considers that

$$dP = \rho_s g dz \quad (3)$$

The melting rate can then be estimated as:

$$\Gamma = \rho_s^2 g W \frac{\mathrm{d}F}{\mathrm{d}P} \quad (4)$$

For the pyroxenite melting scenarios, a non-linear, logarithmic formula was determined to produce the best fit:

$$F = a_{px} \ \ln(P) + b_{px} \quad (5)$$

where a_{px} and b_{px} are the best-fit coefficients for each scenario, given the degree of melting as a function of pressure from the Melt-PX calculations described above.

Hence:

$$\frac{dF}{d\ \ln(P)} = a_{px} \quad (6)$$

$$\frac{dF}{dP} = a_{px}/P \quad (7)$$

The unit of the melting rate is commonly in kg/m^3/yr., but here was converted to melt fraction per unit time to be consistent with the definition of Richardson and McKenzie (1994), using the following equation:

$$\gamma = \Gamma/\rho_s \quad (8)$$

The melt compositions were then integrated over each melting column using a trapezoidal rule adapted for uneven step spacing.

5.2.4. Reactive porous flow calculations of ^{238}U-^{230}Th-^{226}Ra and ^{235}U-^{231}Pa disequilibria

Reactive porous flow melting calculations were conducted in parallel with dynamic melting calculations to allow for direct comparison of results. For RPF model calculations, we used the UserCalc calculator of Spiegelman (2000), a tool that determines U-series isotope disequilibria for a one-dimensional melt column experiencing chromatographic porous flow after Spiegelman and Elliott (1993). All initial activity ratios had a value of 1.0 (i.e., the mantle source started in secular equilibrium prior to melting), the permeability exponent was fixed at a value of 2, and permeability did not change with depth (see Spiegelman, 2000). As with dynamic melting, for each lithology and scenario tested, the degree of melting and bulk partition coefficients were tabulated as a function of depth using results from Sections 5.2.1 and 5.2.2, and were then used as inputs for the RPF model. Both degrees of melting and mineral modes (used to calculate bulk partition coefficients) were drawn from the results of the calculations described above, after Lambart (2017) (see Table S2), with mineral/melt partition coefficients for each lithology drawn from Table 1.

5.2.5. Modeling outcomes

Here we present the primary outcomes and key findings from our models. (A more detailed presentation of our results can be found in the Supplementary Information.) We used dynamic and RPF models to determine (^{230}Th/^{238}U), (^{226}Ra/^{230}Th), and (^{231}Pa/^{235}U) activity ratios for partial melts produced along one-dimensional upwelling melting columns, for each of the lithologies and scenarios described above. We tested a range of solid mantle upwelling velocities and maximum residual melt porosities. Melting was stopped at a final pressure of either 0.5 GPa to simulate mid-ocean ridge environments, or 2.0 GPa to simulate an ocean island setting overlying thicker oceanic lithosphere, after Hole and Millett (2016). The resulting melt compositions from the top of each melt column for each lithology are shown in Figs. S3-S12. As in previous studies, in general higher U-series isotope disequilibria are produced when upwelling rates are low and the maximum residual melt porosity is small, but there is significant variation among the scenarios tested here, and a few outcomes that notably differ from prior studies, as discussed below.

Dynamic melting outcomes for peridotite melting were remarkably consistent for a given potential temperature, across all scenarios (Figs. S3-S4, S8-S12). Depending on upwelling rate and maximum residual porosity, final (^{230}Th/^{238}U) ratios in peridotite partial melts have a very limited range, from secular equilibrium (1.0) to just under 6% ^{230}Th excess relative to ^{238}U for a mantle potential temperature of 1300°C, and just over 3% ^{230}Th excess for a mantle potential temperature of 1550°C. (^{226}Ra/^{230}Th) ratios range up to 3.3 for both temperature scenarios, and (^{231}Pa/^{235}U) up to a maximum of 5.5. Reactive porous flow melting produced similar results for peridotite partial melts with potential temperatures of 1300°C, but the range of (^{230}Th/^{238}U) achieved at higher potential temperatures was notably larger than for dynamic melts (ranging from a ^{230}Th deficit of 5% up to (^{230}Th/^{238}U) = 1.2) (Figs. S5-S6). Scenarios with a deeper final melting pressure of 2.0 GPa were overall similar to final pressures of 0.5 GPa, except that ^{230}Th deficits were not observed (Figs. S7-S8). The most extreme (^{226}Ra/^{230}Th) ratios determined for RPF melting of peridotite ranged up to notably high values of ~7, with (^{231}Pa/^{235}U) up to ~9.

Dynamic melting of pyroxenites also produced relatively consistent results across thermal equilibrium versus isolation scenarios, and for all final melting depths. On the whole, however, pyroxenite partial melts have a much broader range of activity ratios than peridotites (Figs. S3-S4). Melting of either pyroxenite type produced (^{230}Th/^{238}U) between 1.0 and ~1.4 for all temperatures. Predicted (^{226}Ra/^{230}Th) and (^{231}Pa/^{235}U) ratios for pyroxenite melting ranged up to even more extreme values than peridotite partial melts (~9 and ~14, respectively). The consistency of our dynamic melting outcomes, even for different pyroxenite lithologies with distinct modal mineralogy and bulk partition coefficients, indicates that the dynamic melting results are only moderately sensitive to the choice of partition coefficients.

Reactive porous flow melting of pyroxenite produced the most variable outcomes for the scenarios tested, suggesting the RPF model is far

more sensitive to moderate changes in D values than dynamic melting (Figs. S5-S6). At a mantle potential temperature of 1300°C, Gb-108 partial melts exhibited (^{230}Th/^{238}U) ratios between 1.03 and 1.6 in thermal equilibrium with peridotite, and between 0.95 and 1.4 in thermal isolation; (^{226}Ra/^{230}Th) ratios between 0.7 and 3 in thermal equilibrium and 0.35 to 1 in thermal isolation; and (^{231}Pa/^{235}U) from 1.03 to 10.7 in thermal equilibrium and 1.3 to 9.5 in thermal isolation. Melting of MIX1G likewise produced highly variable, but notably different results, with (^{230}Th/^{238}U) of ~1 to ~1.3 in both scenarios, (^{226}Ra/^{230}Th) of 2 to 24 in thermal equilibrium and more moderately high 1.1 to 10 in thermal isolation, and (^{231}Pa/^{235}U) of 1.25 to 19 in thermal equilibrium and 1.5 to 23 in thermal isolation. With the RPF model, thermal equilibration thus produced notably different outcomes for pyroxenite melt compositions. This effect was most detectable for the potential temperatures and pyroxenite lithologies where the impact of thermal equilibration on the degree of melting was greatest, e.g. $T_p = 1550$°C and Gb-108 pyroxenite. The most extreme disequilibrium values are also associated with particularly high porosities and slow upwelling rates. We note that especially high (^{226}Ra/^{230}Th) ratios in basalts similar to those modeled here may be logical outcomes in some circumstances, such as arc-related melting; for example, especially large ^{226}Ra excesses have been observed in some Tonga basalts (Turner et al., 2000).

6. Discussion

Prior research has suggested that near-fractional, dynamic melting of peridotite is sufficient to explain most of the observed isotope disequilibria in MORB (e.g., Stracke et al., 2006). Our modeling results do not corroborate this suggestion. Dynamic melts of peridotite, shown in Figs. S3-S4 and S8-S10, fail to produce most of the compositions observed in global MORB, an outcome that is mostly insensitive to changes in the melting scenario. The relative insensitivity of the model matches expectations, since near-fractional melting is mainly sensitive to initial melting conditions in the deepest part of the melt column (e.g., McKenzie, 1985; Williams and Gill, 1989). Changes such as an increase in the final pressure of melting, or continuous thermal reequilibration between two lithologies, thus have little impact on the aggregated melt composition. In summary, our dynamic melting models produce a notably restricted range of (^{230}Th/^{238}U) ratios in peridotite partial melts, across all conditions tested. This is different from prior findings (e.g., Stracke et al., 2006), where dynamic melting calculations for peridotite source rocks have produced sufficiently high (^{230}Th/^{238}U) to explain most oceanic basalts, and thus warrants further explanation. Some of those prior studies similarly considered the effects of changing partition coefficients during the melt process, using incremental calculations (e.g., Stracke et al., 2003c). Models like dynamic melting may indeed be sensitive to the choice of partition coefficients (e.g., Elkins et al., 2008; Pertermann and Hirschmann, 2003a; Sims et al., 2002), and prior work has tested a range of values based on the experimental data thought to be the most appropriate at the time; but our precise choice of mineral/melt partition coefficient values (Table 1) and initial peridotite mineral modes (Table S2) can only explain moderate differences in final (^{230}Th/^{238}U) ratios, and not the restricted range of our results. Indeed, and as noted above, the similarity in outcomes for our pyroxenite dynamic melting calculations, even across different lithologies with distinct mineral/melt partition coefficients and mineral modes, suggests our dynamic melting results have only limited sensitivity to bulk partitioning properties. We instead interpret the particularly low and consistent (^{230}Th/^{238}U) in our peridotite dynamic melting results as primarily a product of varying melt productivity during the early melting process in the dynamic melting environment, as this constitutes the most significant difference between our methods and prior research. That is, while initial, very low-degree melting steps must produce significant (^{230}Th/^{238}U) in an instantaneous melt, the thermodynamically-constrained productivity variations predicted by Melt-PX (Lambart et al., 2016) result in far more immediate dilution of the aggregated liquid by instantaneous liquids with lower (^{230}Th/^{238}U), due to the rapidly increasing melting rate early in the melting process.

We consider this outcome to be a significant finding that argues against purely dynamic melting of peridotite mantle to explain the vast majority of global oceanic basalts, which largely have higher (^{230}Th/^{238}U) than our model outcomes. While near-fractional melting and channelized melt transport likely play an important role during mantle melting (e.g., Kelemen et al., 1997), it thus cannot be the *only* melting and melt transport regime involved in most settings. In a relatively *homogeneous* mantle dominated by peridotite melting, the best remaining explanations for high (^{230}Th/^{238}U) ratios in basalts are 1) RPF melting at even slower upwelling rates (e.g., < 1 cm/yr.) (Figs. S5-S6); and 2) two-porosity flow, where efficient extraction of deeper melts with high (^{230}Th/^{238}U) occurs via channelized flow (roughly equivalent to a dynamic melt), while magmas with low (^{230}Th/^{238}U) can be explained by shallower extraction along a lower-porosity, RPF pathway. This finding agrees with prior work (e.g., Jull et al., 2002; Sims et al., 2002) (see Supplementary Information). In regions with independent geochemical evidence for greater mantle heterogeneity (e.g., varying radiogenic isotope ratios) or high upwelling rates, however, our model results further support an alternate source of high (^{230}Th/^{238}U) that is of greater interest to the questions investigated here, namely pyroxenite melting within a lithologically heterogeneous mantle source region.

Although all model results are shared in Figs. S3-S12 for completeness, we logically constrain our results for pyroxenite involvement in mantle melting based on expected external limitations. As noted above, thermal equilibration with ambient peridotite can affect the U-series disequilibria produced during partial melting, and we expect such equilibration to largely occur except for the largest-diameter heterogeneities in the mantle (> 10 km) (Kogiso et al., 2004b). As such, we can consider the effects of thermally isolated melting of pyroxenite under typical mantle conditions as less likely. We also assume that near-fractional, efficient extraction and transport via channelized flow is the dominant mechanism for pyroxenite partial melting in a dominantly peridotitic mantle. Partial melting of pyroxenite heterogeneities is likely to form high porosity channels in which pyroxenite melts can be efficiently segregated and rapidly transported to the surface (e.g., Weatherley and Katz, 2012), as thermal diffusion from peridotite to pyroxenite-rich channels prevents melting and efficient drainage of rocks adjacent to channels. Pyroxenite partial melts that do travel by porous flow would likely react with surrounding peridotite and freeze (e.g., Lambart et al., 2012; Yaxley and Green, 1998), producing hybridized rocks. Hence, extracted partial melts of *pyroxenite* should be dominantly the product of *dynamic melting* and channelized transport, while partial melts of peridotite are more likely to experience porous flow, per the discussion above. This expectation is supported by significant mismatches observed between some of our RPF modeling outcomes for pyroxenite melting and the global oceanic basalt data set. In particular, we calculated large ^{226}Ra deficits relative to ^{230}Th in RPF melts of Gb-108, due to the predicted presence of stable plagioclase in silica-rich eclogite under mantle conditions and resulting relatively high bulk Ra partition coefficients. Such deficits are generally not observed in MORB or OIB (Figs. 3-4, Table S1).

Fig. 7a-b shows a restricted set of model outcomes likely to resemble melt generation in a MORB setting, focusing on solid mantle upwelling rates between 1 and 10 cm/yr. To simulate the likely different transport mechanisms expected for depleted, peridotite-derived and enriched, pyroxenite-derived partial melts in a two-lithology melting regime, we show low-porosity (0.1 to 0.5 %) RPF peridotite melts in blue with higher-porosity (0.5 to 1.0 %) dynamic melts of the two pyroxenite lithologies in red (Gb-108) and maroon (MIX1G). All model results shown in Fig. 7 also assume thermal equilibrium between chemically isolated heterogeneous lithologies. We restrict peridotite melting to porous flow scenarios due to the restricted range of dynamic melts observed above, as well as the likelihood of two porosity transport in a

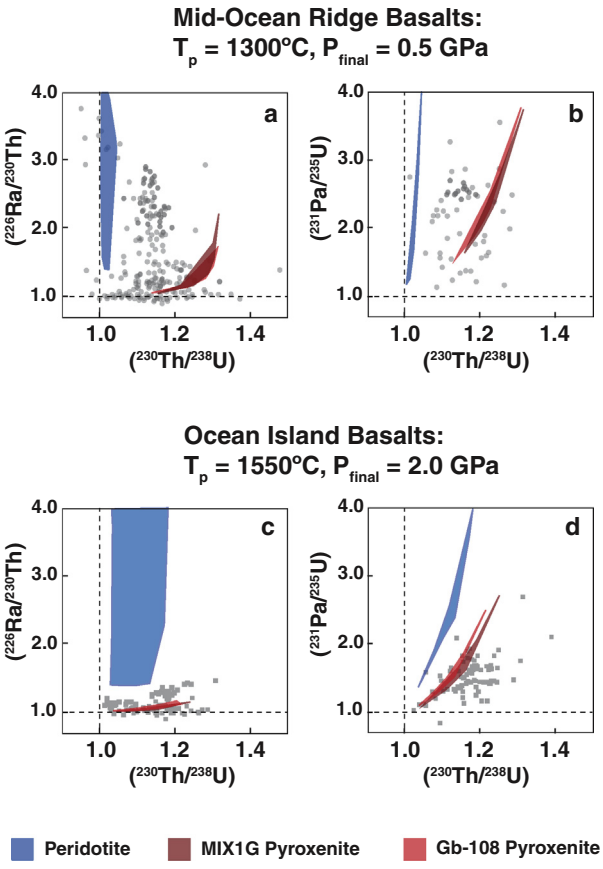

Fig. 7. Summary highlighting key results of melt modeling calculations for peridotite (blue fields), Gb-108 pyroxenite (red fields), and MIX1G pyroxenite lithologies (maroon fields). a. ($^{226}Ra/^{230}Th$) vs. ($^{230}Th/^{238}U$) and b. ($^{231}Pa/^{235}U$) vs. ($^{230}Th/^{238}U$) for scenarios relevant to MORB melt generation, with a mantle potential temperature of 1300°C and a final melting pressure of 0.5 GPa. All model results shown assume full thermal equilibrium between coexisting lithologies. Peridotite melting results shown cover a range of solid mantle upwelling rates from 1 to 10 cm/yr. and residual melt porosities of 0.1 to 0.5 % for RPF melting, while pyroxenite melting calculations use the same solid mantle upwelling rates with higher porosities of 0.5 to 1.0 % in a dynamic melting scenario. Global MORB data after Fig. 3 are shown in gray. c. ($^{226}Ra/^{230}Th$) vs. ($^{230}Th/^{238}U$) and d. ($^{231}Pa/^{235}U$) vs. ($^{230}Th/^{238}U$) for OIB melting at a mantle potential temperature of 1550°C and final melting pressure of 2.0 GPa. Model scenarios shown are similar to those in panels (a)and (b), except solid mantle upwelling rates shown are restricted to 5 to 50 cm/yr. Global OIB data after Fig. 4 are shown in gray.

lithologically heterogeneous mantle. A range of mixtures of melts derived from the peridotite and pyroxenite fields is possible, and could readily explain the majority of the observed MORB data, shown in gray.

The highest ($^{230}Th/^{238}U$) and lowest ($^{231}Pa/^{235}U$) disequilibrium values observed in MORB are less well explained, however, particularly considering the relative insensitivity of the dynamic melting results to changes in pyroxenite bulk mineralogy and partition coefficients (Fig. 7b). In fact, none of our calculated melt compositions for T_p = 1300°C can fully explain the most extreme observed basalts in Fig. 7b. One scenario that could generate magmas in this field is increasing the time of melt extraction after segregation into a disequilibrium melt channel, e.g. after Stracke et al. (2006), which could moderately reduce the ($^{231}Pa/^{235}U$) ratio but would have little effect on ($^{230}Th/^{238}U$). In a number of locations, however, the aging expected to occur during transport or storage has been insufficient to explain systematically low ($^{226}Ra/^{230}Th$) or ($^{231}Pa/^{235}U$) in measured basalts (e.g., Jan Mayen Island; Elkins et al., 2016). Alternatively, the basalts with particularly high ($^{230}Th/^{238}U$) and low ($^{231}Pa/^{235}U$) may derive from regions with locally hotter mantle potential temperatures, causing them to more closely resemble hotspot-derived basalts.

For OIB scenarios, we similarly restricted the model outcomes we considered relevant in Fig. 7c-d, but for a higher mantle potential temperature of 1550°C, solid mantle upwelling rates of 5 to 50 cm/yr., and a final melting pressure of 2.0 GPa to simulate thicker oceanic lithosphere for all model scenarios. Although again, mixtures between peridotite and pyroxenite partial melts could generate much of the observed data, here the mismatch in ($^{231}Pa/^{235}U$) vs. ($^{230}Th/^{238}U$) between model outcomes and measured basalts is greater than it was for MORB. While segregated magma must travel from the base of the lithosphere at 2.0 GPa to the surface in this scenario, allowing for greater decay during transport, the mismatch is large enough to make this a less satisfactory explanation. However, unlike at the lower potential temperatures in Fig. 7b, under hotter conditions there is a greater range of possible model outcomes for pyroxenite melting (Figs. S3-S12), some of which could generate magmas with sufficiently high ($^{230}Th/^{238}U$) and sufficiently low ($^{231}Pa/^{235}U$) to explain the observed data. For example, if a small portion of pyroxenitic partial melts were in fact transported by reactive porous flow, or if some pyroxenite heterogeneities were sufficiently large to remain thermally isolated during melting, much of the mismatch could be overcome.

While our preliminary modeling outcomes neither exhaust all possible scenarios, nor provide a perfect fit to the global oceanic basalt data set, they are encouraging. In particular, they demonstrate that pure peridotite melting is insufficient to generate the vast majority of global oceanic basalts, and show that at least a small contribution of partial melts from pyroxenitic lithologies is likely. However, we judge it unlikely that most mantle melting regimes are dominated by a *purely* pyroxenitic source, even if that source is the product of hybridization, as suggested by Sobolev et al. (2005). Instead, we favor variable extents of mixing of the partial melts produced by a range of lithologic types and melting processes. In such a scenario, the relatively high trace element content of enriched pyroxenites allows the pyroxenite melts to more strongly influence the resulting composition of the aggregate than the proportion of pyroxenite in the source region would suggest (e.g., Sims et al., 2013; Stracke et al., 1999). Such magma mixing processes could produce a large range of aggregated melt compositions, depending on the precise pyroxenite composition, pyroxenite abundance, thermal conditions, channel density, and upwelling rate of the mantle regime. In some regions (e.g., 9-10°N EPR; Sims et al., 2002), pyroxenite presence is limited in size and abundance, such that compositions may effectively mimic the melting of a homogeneous source, with limited channel production and a stronger influence by porous flow processes. In others (e.g., Jan Mayen Island; Elkins et al., 2016), larger and/or more abundant pyroxenite heterogeneities strongly influence the formation and density of channels, alongside a range of porous-flow or dynamic melting processes within the dominant peridotite rocks. We believe this model largely explains the global production of OIB and MORB and corroborates the majority of oceanic basalt U-series disequilibrium data from the literature, although more exotic or unusual conditions may persist in limited regions. Our updated and synthesized modeling results generally support a widespread and important role for pyroxenite melting in most mantle melting regimes.

7. Conclusions

Based on our synthesis of U-series disequilibrium analysis in basalts and its efficacy as a technique for investigating mantle lithologic heterogeneity, we can address the two questions posed in the introduction to this paper:

1) How are U-series isotopes a useful tool for investigating the nature and magnitude of mantle lithologic heterogeneity?

   Uranium-series isotopic disequilibria remain the primary source of information about the timescales of partial melting in the mantle, which is in turn the main mechanism whereby new oceanic crust

is formed on Earth; as such, they continue to be a key approach for understanding how processes like plate tectonics, mantle convection, and large scale chemical recycling interact. Thus, U-series isotopes remain a necessary and relevant method for evaluating the igneous petrogenesis of young, fresh lavas. In addition, the synthesis of forward modeling techniques demonstrated here corroborates recent studies suggesting that U-series disequilibrium analysis is a sensitive indicator of the involvement of pyroxenite in mantle melting, in ways that differ from other geochemical indicators of lithologic variations in the melt source. Those indicators, based on our synthesis of modeling efforts, broadly support a widespread role for pyroxenite in most upper mantle melting regimes.

2) How has this technique helped our understanding of mantle makeup and melt generation to-date, and where might the geochemical community best concentrate its future efforts?
The range of U-series isotope disequilibria observed in global oceanic basalts, particularly when considered with additional geochemical indicators of heterogeneity, generally supports the involvement of pyroxenite in the partial melting of the sub-oceanic mantle. Additionally, while pyroxenite melting should be largely dominated by dynamic melting processes and channelized melt transport, reactive porous flow and two-porosity transport regimes for peridotite melt are likely necessary to fully explain U series isotope systematics, with or without local heterogeneity effects.

When assessing the nature of the partial melting process using forward melting model calculations, non-linear variations in melt productivity during the melting process, continuous changes in partition coefficients due to changing mineral modes, and thermal equilibration between melting pyroxenites and ambient mantle peridotite rocks should all be taken into account; though thermal equilibration likely plays a more minor role, in light of the dominantly dynamic melting of pyroxenites, which is relatively insensitive to such effects. The presence of lithospheric lids beneath hotspots should also be considered for peridotite melting by RPF, where such lids can have a notable effect. We generally encourage researchers to evaluate both RPF and dynamic melting of peridotite, and to utilize available numerical solutions for both models to most accurately assess the competing effects of the variables listed above.

Supplementary data to this article can be found online at https://doi.org/10.1016/j.lithos.2019.02.011.

Acknowledgments

We are grateful to the editors of *Lithos* for inviting us to write this review article. We thank K. Sims and M. Spiegelman for thoughtful discussions related to this manuscript. We also thank two anonymous reviewers for their constructive comments that helped to improve the manuscript. S.L. acknowledges funding support from NSF grant EAR-1834367.

References

van Acken, D., Becker, H., Walker, R.J., 2008. Refertilization of Jurassic oceanic peridotites from the Tethys Ocean—implications for the Re–Os systematics of the upper mantle. Earth and Planetary Science Letters 268, 171–181.

Aharonov, E., Spiegelman, M., Kelemen, P., 1997. Three-dimensional flow and reaction in porous media: Implications for the Earth's mantle and sedimentary basins. Journal of Geophysical Research - Solid Earth 102, 14821–14833.

Allègre, C., 1968. ^{230}Th dating of volcanic rocks: a comment. Earth and Planetary Science Letters 5, 209–210.

Allègre, C.J., Condomines, M., 1982. Basalt genesis and mantle structure studied through Th-isotopic geochemistry. Nature 299, 21–24.

Allègre, C.J., Hamelin, B., Dupré, B., 1984. Statistical analysis of isotopic ratios in MORB: the mantle blob cluster model and the convective regime of the mantle. Earth and Planetary Science Letters 71, 71–84.

Asimow, P.D., Hirschmann, M., Ghiorso, M., O'Hara, M., Stolper, E., 1995. The effect of pressure-induced solid-solid phase transitions on decompression melting of the mantle. Geochimica et Cosmochimica Acta 59, 4489–4506.

Asimow, P.D., Hirschmann, M.M., Stolper, E.M., 2001. Calculation of peridotite partial melting from thermodynamic models of minerals and melts. IV. Adiabatic decompression and the composition and mean properties of mid-ocean ridge basalts. Journal of Petrology 42, 963–998.

Asimow, P.D., Dixon, J., Langmuir, C., 2004. A hydrous melting and fractionation model for mid-ocean ridge basalts: application to the Mid-Atlantic Ridge near the Azores. Geochemistry, Geophysics, Geosystems 5. https://doi.org/10.1029/2003GC000568.

Beattie, P., 1993. Uranium Thorium Disequilibria and Partitioning on Melting of Garnet Peridotite. Nature 363, 63–65.

Ben Othman, D., Allègre, C., 1990. Th isotopic systematics at 13° N east Pacific Ridge segment. Earth and Planetary Science Letters 98, 129–137.

Bickle, M., McKenzie, D., 1987. The transport of heat and matter by fluids during metamorphism. Contributions to Mineralogy and Petrology 95, 384–392.

Blichert-Toft, J., Albarede, F., Kornprobst, J., 1999. Lu-Hf isotope systematics of garnet pyroxenites from Beni Bousera, Morocco: Implications for basalt origin. Science 283, 1303–1306.

Blundy, J.D., Wood, B.J., 2003. Mineral-melt partitioning of uranium, thorium, and their daughters. Reviews in Mineralogy 59–123.

Borghini, G., Fumagalli, P., Rampone, E., 2017. Partial melting of secondary pyroxenite at 1 and 1.5 GPa, and its role in upwelling heterogeneous mantle. Contributions to Mineralogy and Petrology 172, 70. https://doi.org/10.1007/s00410-017-1387-4.

Bourdon, B., Sims, K.W., 2003. U-series constraints on intraplate basaltic magmatism. Reviews in Mineralogy and Geochemistry 52, 215–254.

Bourdon, B., Langmuir, C.H., Zindler, A., 1996a. Ridge-hotspot interaction along the Mid-Atlantic Ridge between 37 degrees 30' and 40 degrees 30'N: The U-Th disequilibrium evidence. Earth and Planetary Science Letters 142, 175–189.

Bourdon, B., Zindler, A., Elliott, T., Langmuir, C.H., 1996b. Constraints on mantle melting at mid-ocean ridges from global U-238-Th-230 disequilibrium data. Nature 384, 231–235.

Bourdon, B., Joron, J.L., Claude-Ivanaj, C., Allegre, C.J., 1998. U-Th-Pa-Ra systematics for the Grande Comore volcanics: melting processes in an upwelling plume. Earth and Planetary Science Letters 164, 119–133.

Bourdon, B., Goldstein, S.J., Bourles, D., Murrell, M.T., Langmuir, C.H., 2000. Evidence from ^{10}Be and U series disequilibria on the possible contamination of mid-ocean ridge basalt glasses by sedimentary material. Geochemistry, Geophysics, Geosystems 1 (2000GC000047).

Bourdon, B., Turner, S.P., Henderson, G.M., Lundstrom, C.C., 2003. Introduction to U-series geochemistry. In: Bourdon, B., Henderson, G.M., Lundstrom, C.C., Turner, S.P. (Eds.), Uranium-Series Geochemistry. Mineralogical Society of America, Washington, D.C., pp. 1–21.

Bourdon, B., Turner, S.P., Ribe, N.M., 2005. Partial melting and upwelling rates beneath the Azores from a U-series isotope perspective. Earth and Planetary Science Letters 239, 42–56.

Bourdon, B., Ribe, N.M., Stracke, A., Saal, A.E., Turner, S.P., 2006. Insights into the dynamics of mantle plumes from uranium-series geochemistry. Nature 444, 713–717.

Bown, J.W., White, R.S., 1994. Variation with spreading rate of oceanic crustal thickness and geochemistry. Earth and Planetary Science Letters 121, 435–449.

Brunelli, D., Seyler, M., Cipriani, A., Ottolini, L., Bonatti, E., 2005. Discontinuous melt extraction and weak refertilization of mantle peridotites at the Vema lithospheric section (Mid-Atlantic Ridge). Journal of Petrology 47, 745–771.

Brunelli, D., Cipriani, A., Bonatti, E., 2018. Thermal effects of pyroxenites on mantle melting below mid-ocean ridges. Nature Geoscience 1, 520–525.

Chabaux, F., Allègre, C.J., 1994. U-238 Th-230-Ra-226 Disequilibria in Volcanics - a New Insight into Melting Conditions. Earth and Planetary Science Letters 126, 61–74.

Chase, C.G., 1981. Oceanic island Pb: two-stage histories and mantle evolution. Earth and Planetary Science Letters 52, 277–284.

Chazot, G., Charpentier, S., Kornprobst, J., Vannucci, R., Luais, B., 2005. Lithospheric mantle evolution during continental break-up: the West Iberia non-volcanic passive margin. Journal of Petrology 46, 2527–2568.

Claude-Ivanaj, C., Bourdon, B., Allegre, C.J., 1998. Ra-Th-Sr isotope systematics in Grande Comore Island: a case study of plume-lithosphere interaction. Earth and Planetary Science Letters 164, 99–117.

Claude-Ivanaj, C., Joron, J.L., Allegre, C.J., 2001. U-238-Th-230-Ra-226 fractionation in historical lavas from the Azores: long-lived source heterogeneity vs. metasomatism fingerprints. Chemical Geology 176, 295–310.

Cohen, A.S., O'Nions, R.K., 1993. Melting rates beneath Hawaii: evidence from uranium series isotopes in recent lavas. Earth and Planetary Science Letters 120, 169–175.

Condomines, M., Morand, P., Allegre, C.J., 1981. ^{230}Th-^{238}U radioactive disequilibria in tholeiites from the FAMOUS zone (Mid-Atlantic Ridge, 36°50'N): Th and Sr isotopic geochemistry. Earth and Planetary Science Letters 55, 247–256.

Condomines, M., Gauthier, P.-J., Sigmarsson, O., 2003. Timescales of magma chamber processes and dating of young volcanic rocks. In: Bourdon, B., Henderson, G.M., Lundstrom, C.C., Turner, S.P. (Eds.), Uranium-Series Geochemistry. Mineralogical Society of America, Washington, DC, pp. 125–174.

Constantin, M., Hékinian, R., Ackermand, D., Stoffers, P., 1995. Mafic and ultramafic intrusions into upper mantle peridotites from fast spreading centers of the Easter Microplate (South East Pacific), Mantle and lower crust exposed in oceanic ridges and in ophiolites. Springer, pp. 71–120.

Coogan, L., O'Hara, M., 2015. MORB differentiation: In situ crystallization in replenished-tapped magma chambers. Geochimica et Cosmochimica Acta 158, 147–161.

Cooper, K.M., Goldstein, S.J., Sims, K.W.W., Murrell, M.T., 2003. Uranium-series chronology of Gorda Ridge volcanism: new evidence from the 1996 eruption. Earth and Planetary Science Letters 206, 459–475.

Daines, M.J., Kohlstedt, D.L., 1994. The transition from porous to channelized flow due to melt/rock reaction during melt migration. Geophysical Research Letters 21, 145–148.

Dantas, C., Ceuleneer, G., Gregoire, M., Python, M., Freydier, R., Warren, J., Dick, H., 2007. Pyroxenites from the Southwest Indian Ridge, 9–16 E: cumulates from incremental

melt fractions produced at the top of a cold melting regime. Journal of Petrology 48, 647–660.
Davis, F.A., Humayun, M., Hirschmann, M.M., Cooper, R.S., 2013. Experimentally determined mineral/melt partitioning of first-row transition elements (FRTE) during partial melting of peridotite at 3 GPa. Geochimica et Cosmochimica Acta 104, 232–260.
Day, J.M., Pearson, D.G., Macpherson, C.G., Lowry, D., Carracedo, J.-C., 2009. Pyroxenite-rich mantle formed by recycled oceanic lithosphere: Oxygen-osmium isotope evidence from Canary Island lavas. Geology 37, 555–558.
Dick, H.J.B., Lissenberg, C.J., Warren, J.M., 2010. Mantle melting, melt transport, and delivery beneath a slow-spreading ridge: The paleo-MAR from 23°15'N to 23°45'N. Journal of Petrology 51, 425–467.
Downes, H., 2007. Origin and significance of spinel and garnet pyroxenites in the shallow lithospheric mantle: Ultramafic massifs in orogenic belts in Western Europe and NW Africa. Lithos 99, 1–24.
Elkins, L.J., Gaetani, G.A., Sims, K.W.W., 2008. Partitioning of U and Th during garnet pyroxenite partial melting: Constraints on the source of alkaline ocean island basalts. Earth and Planetary Science Letters 265, 270–286.
Elkins, L.J., Sims, K.W.W., Prytulak, J., Mattielli, N., Elliott, T., Blichert-Toft, J., Blusztajn, J., Dunbar, N., Devey, C.W., Mertz, D.F., Schilling, J.G., 2011. Understanding melt generation beneath the slow spreading Kolbeinsey Ridge from ^{238}U, ^{230}Th, and ^{231}Pa excesses. Geochimica et Cosmochimica Acta 75, 6300–6329.
Elkins, L.J., Sims, K.W.W., Prytulak, J., Blichert-Toft, J., Elliott, T., Blusztajn, J., Fretzdorff, S., Reagan, M., Haase, K., Humphris, S., Schilling, J.G., 2014. Melt generation beneath Arctic Ridges: Implications from U decay series disequilibria in the Mohns, Knipovich, and Gakkel Ridges. Geochimica et Cosmochimica Acta 127, 140–170.
Elkins, L.J., Scott, S.R., Sims, K.W.W., Rivers, E.R., Devey, C.W., Reagan, M., Hamélin, C., Pedersen, R., 2016. Exploring the role of mantle eclogite at mid-ocean ridges and hotspots: U-series constraints on Jan Mayen Island and the Kolbeinsey Ridge. Chemical Geology 444, 128–140.
Elkins-Tanton, L.T., Foulger, G., 2005. Continental magmatism caused by lithospheric delamination. Special Papers-Geological Society of America. 388, p. 449.
Elliott, T., 1997. Fractionation of U and Th during mantle melting: a reprise. Chemical Geology 139, 165–183.
Fabbrizio, A., Schmidt, M.W., Günther, D., Eikenberg, J., 2009. Experimental determination of Ra mineral/melt partitioning for feldspars and 226Ra-disequilibrium crystallization ages of plagioclase and alkali-feldspar. Earth and Planetary Science Letters 280, 137–148.
Faul, U.H., 2001. Melt retention and segregation beneath mid-ocean ridges. Nature 410, 920–923.
Faure, G., Mensing, T.M., 2005. Isotopes: Principles and Applications. 3rd ed. John Wiley and Sons, Inc, Hoboken, New Jersey.
Ghiorso, M.S., Hirschmann, M.M., Reiners, P.W., Kress, V.C., 2002. The pMELTS: A revision of MELTS for improved calculation of phase relations and major element partitioning related to partial melting of the mantle to 3 GPa. Geochemistry, Geophysics, Geosystems 3, 1–35.
Godard, M., Lagabrielle, Y., Alard, O., Harvey, J., 2008. Geochemistry of the highly depleted peridotites drilled at ODP Sites 1272 and 1274 (Fifteen-Twenty Fracture Zone, Mid-Atlantic Ridge): Implications for mantle dynamics beneath a slow spreading ridge. Earth and Planetary Science Letters 267, 410–425.
Goldstein, S.J., Murrell, M.T., Jackecky, D.R., 1989. Th and U isotopic systematics of basalts from the Juan de Fuca and Gorda Ridges by mass spectrometry. Earth and Planetary Science Letters 96, 134–146.
Goldstein, S.J., Murrell, M.T., Janecky, D.R., Delaney, J.R., Clague, D.A., 1991. Geochronology and petrogenesis of morb from the Juan-De-Fuca and Gorda Ridges by U-238 Th-230 disequilibrium. Earth and Planetary Science Letters 109, 255–272.
Goldstein, S.J., Murrell, M.T., Janecky, D.R., Delaney, J.R., Clague, D.A., 1992. Geochronology and petrogenesis of morb from the Juan-De-Fuca and Gorda Ridges by U-238 Th-230 disequilibrium. Earth and Planetary Science Letters 109, 255–272.
Goldstein, S.J., Murrell, M.T., Williams, R.W., 1993. Pa-231 and Th-230 chronology of Midocean Ridge Basalts. Earth and Planetary Science Letters 115, 151–159.
Gurenko, A.A., Sobolev, A.V., Hoernle, K.A., Hauff, F., Schmincke, H.U., 2009. Enriched, HIMU-type peridotite and depleted recycled pyroxenite in the Canary plume: a mixed-up mantle. Earth and Planetary Science Letters 277, 514–524.
Halliday, A.N., Lee, D.-C., Tommasini, S., Davies, G.R., Paslick, C.R., Fitton, J.G., James, D.E., 1995. Incompatible trace elements in OIB and MORB and source enrichment in the sub-oceanic mantle. Earth and Planetary Science Letters 133, 379–395.
Harvey, J., Gannoun, A., Burton, K.W., Rogers, N.W., Alard, O., Parkinson, I.J., 2006. Ancient melt extraction from the oceanic upper mantle revealed by Re–Os isotopes in abyssal peridotites from the Mid-Atlantic ridge. Earth and Planetary Science Letters 244, 606–621.
Hauri, E., Hart, S., 1993. Re-Os isotope systematics of HIMU and EMII oceanic island basalts from the south Pacific Ocean. Earth and Planetary Science Letters 114, 353–371.
Hauri, E., Whitehead, J.A., Hart, S.R., 1994a. Fluid dynamic and geochemical aspects of entrainment in mantle plumes. Journal of Geophysical Research - Solid Earth 99, 24275–24300.
Hauri, E.H., Wagner, T.P., Grove, T.L., 1994b. Experimental and Natural Partitioning of Th, U, Pb and Other Trace-Elements between Garnet, Clinopyroxene and Basaltic Melts. Chemical Geology 117, 149–166.
Hébert, R., Gueddari, K., Lafleche, M., Beslier, M.-O., Gardien, V., 2001. Petrology and geochemistry of exhumed peridotites and gabbros at non-volcanic margins: ODP Leg 173 West Iberia ocena-continent transition zone. Geological Society, London, Special Publications 187, 161–189.
Hellebrand, E., Snow, J.E., Muhe, R., 2002. Mantle melting beneath Gakkel Ridge (Arctic Ocean): abyssal peridotite spinel compositions. Chemical Geology 182, 227–235.
Herzberg, C., 2006. Petrology and thermal structure of the Hawaiian plume from Mauna Kea volcano. Nature 444, 605–609.
Herzberg, C., 2010. Identification of source lithology in the Hawaiian and Canary Islands: Implications for origins. Journal of Petrology 52, 113–146.
Hewitt, I.J., 2010. Modelling melting rates in upwelling mantle. Earth and Planetary Science Letters 300, 264–274.
Hirschmann, M.M., Stolper, E.M., 1996. A possible role for garnet pyroxenite in the origin of the "garnet signature" in MORB. Contributions to Mineralogy and Petrology 124, 185–208.
Hirschmann, M.M., Kogiso, T., Baker, M.B., Stolper, E.M., 2003. Alkalic magmas generated by partial melting of garnet pyroxenite. Geology 31, 481–484.
Hofmann, A., 1997. Mantle geochemistry: the message from oceanic volcanism. Nature 385, 219–229.
Hofmann, A.W., 2007. Sampling mantle heterogeneity through oceanic basalts: Isotopes and trace elements, Treatise on Geochemistry. pp. 1–44.
Hofmann, A.W., White, W.M., 1982. Mantle plumes from ancient oceanic crust. Earth and Planetary Science Letters 57, 421–436.
Hole, M.J., Millett, J.M., 2016. Controls of Mantle Potential Temperature and Lithospheric Thickness on Magmatism in the North Atlantic Igneous Province. Journal of Petrology 57, 417–436.
Humayun, M., Qin, L., Norman, M.D., 2004. Geochemical evidence for excess iron in the mantle beneath Hawaii. Science 306, 91–94.
Ishii, M., Tromp, J., 1999. Normal-mode and free-air gravity constraints on lateral variations in velocity and density of Earth's mantle. Science 285, 1231–1236.
Ito, G., Mahoney, J.J., 2005a. Flow and melting of a heterogeneous mantle: 1. Method and importance to the geochemistry of ocean island and mid-ocean ridge basalts. Earth and Planetary Science Letters 230, 29–46.
Ito, G., Mahoney, J.J., 2005b. Flow and melting of a heterogeneous mantle: 2. Implications for a chemically nonlayered mantle. Earth and Planetary Science Letters 230, 47–63.
Jull, M., Kelemen, P., 2001. On the conditions for lower crustal convective instability. Journal of Geophysical Research - Solid Earth 106, 6423–6446.
Jull, M., Kelemen, P., Sims, K., 2002. Consequences of diffuse and channelled porous melt migration on uranium series disequilibria. Geochimica et Cosmochimica Acta 66, 4133–4148.
Kaneshima, S., Helffrich, G., 1999. Dipping low-velocity layer in the mid-lower mantle: evidence for geochemical heterogeneity. Science 283, 1888–1892.
Katz, R.F., Weatherley, S.M., 2012. Consequences of mantle heterogeneity for melt extraction at mid-ocean ridges. Earth and Planetary Science Letters 335-336, 226–237.
Kay, R.W., Kay, S.M., 1993. Delamination and delamination magmatism. Tectonophysics 219, 177–189.
van Keken, P.E., Hauri, E.H., Ballentine, C.J., 2002. Mantle mixing: the generation, preservation, and destruction of chemical heterogeneity. Annual Review of Earth and Planetary Sciences 30, 493–525.
Kelemen, P.B., Hirth, G., Shimizu, N., Spiegelman, M., Dick, H.J.B., 1997. A review of melt migration processes in the adiabatically upwelling mantle beneath oceanic spreading ridges. Philosophical Transactions of the Royal Society of London Series a-Mathematical Physical and Engineering Sciences 355, 283–318.
Kellogg, L., Turcotte, D., 1990. Mixing and the distribution of heterogeneities in a chaotically convecting mantle. Journal of Geophysical Research - Solid Earth 95, 421–432.
Kempton, P.D., Stephens, C.J., 1997. 16. Petrology and geochemistry of nodular websterite inclusions in harzburgite, Hole 920D1. Kerr, A.C., Saunders, A.D., Tarney, J., Berry, N.H., Hards, V.L., 1995. Depleted mantle-plume geochemical signatures: No paradox for plume theories. Geology 23, 843–846.
Kerr, A.C., Saunders, A.D., Tarney, J., Berry, N.H., Hards, V.L., 1995. Depleted mantle-plume geochemical signatures: No paradox for plume theories. Geology 23, 843–846.
Klemme, S., Günther, D., Hametner, K., Prowatke, S., Zack, T., 2006. The partitioning of trace elements between ilmenite, ulvospinel, armalcolite and silicate melts with implications for the early differentiation of the moon. Chemical Geology 234, 251–263.
Kogiso, T., Hirschmann, M.M., Frost, D.J., 2003. High-pressure partial melting of garnet pyroxenite: possible mafic lithologies in the source of ocean island basalts. Earth and Planetary Science Letters 216, 603–617.
Kogiso, T., Hirschmann, M.M., Pertermann, M., 2004a. High-pressure partial melting of mafic lithologies in the mantle. Journal of Petrology 45, 2407–2422.
Kogiso, T., Hirschmann, M.M., Reiners, P.W., 2004b. Length scales of mantle heterogeneities and their relationship to ocean island basalt geochemistry. Geochimica et Cosmochimica Acta 68, 345–360.
Kokfelt, T.F., Hoernle, K., Hauff, F., 2003. Upwelling and melting of the Iceland plume from radial variation of U-238-Th-230 disequilibria in postglacial volcanic rocks. Earth and Planetary Science Letters 214, 167–186.
Kokfelt, T.F., Lundstrom, C., Hoernle, K., Hauff, F., Werner, R., 2005. Plume-ridge interaction studied at the Galapagos spreading center: Evidence from Ra-226-Th-230-U-238 and Pa-231-U-235 isotopic disequilibria. Earth and Planetary Science Letters 234, 165–187.
Koornneef, J.M., Stracke, A., Bourdon, B., Gronvold, K., 2012. The influence of source heterogeneity on the U-Th-Pa-Ra disequilibria in post-glacial tholeiites from Iceland. Geochimica et Cosmochimica Acta 87, 243–266.
La Tourette, T.Z., Kennedy, A.K., Wasserburg, G.J., 1993. Thorium-uranium fractionation by garnet: Evidence for a deep source and rapid rise of oceanic basalts. Science 261, 729–742.
Lambart, S., 2017. No direct contribution of recycled crust in Icelandic basalts. Geochemical Perspectives Letters 4, 7–12.
Lambart, S., Laporte, D., Schiano, P., 2009. An experimental study of focused magma transport and basalt–peridotite interactions beneath mid-ocean ridges: implications for the generation of primitive MORB compositions. Contributions to Mineralogy and Petrology 157, 429–451.

Lambart, S., Laporte, D., Provost, A., Schiano, P., 2012. Fate of pyroxenite-derived melts in the peridotitic mantle: thermodynamic and experimental constraints. Journal of Petrology 53, 451–476.

Lambart, S., Laporte, D., Schiano, P., 2013. Markers of the pyroxenite contribution in the major-element compositions of oceanic basalts: Review of the experimental constraints. Lithos 160-161, 14–36.

Lambart, S., Baker, M.B., Stolper, E.M., 2016. The role of pyroxenite in basalt genesis: Melt-PX, a melting parameterization for mantle pyroxenites between 0.9 and 5 GPa. Journal of Geophysical Research - Solid Earth 121, 5708–5735.

Langmuir, C., Klein, E.M., Plank, T., 1992. Petrological systematics of mid-ocean ridge basalts: constraints on melt generation beneath ocean ridges. Mantle Flow and Melt Generation at Mid-Ocean Ridges, pp. 183–280.

Lassiter, J.C., Hauri, E.H., Reiners, P.W., Garcia, M.O., 2000. Generation of Hawaiian post-erosional lavas by melting of a mixed lherzolite/pyroxenite source. Earth and Planetary Science Letters 178, 269–284.

Le Roux, P., le Roex, A., Schilling, J.-G., 2002. MORB melting processes beneath the southern Mid-Atlantic Ridge (40–55 S): a role for mantle plume-derived pyroxenite. Contributions to Mineralogy and Petrology 144, 206–229.

Le Roux, V., Lee, C.T., Turner, S.J., 2010. Zn/Fe systematics in mafic and ultramafic systems: Implications for detecting major element heterogeneities in the Earth's mantle. Geochimica et Cosmochimica Acta 74, 2779–2796.

Le Roux, V., Dasgupta, R., Lee, C.T., 2011. Mineralogical heterogeneities in the Earth's mantle: constraints from Mn, Co, Ni and Zn partitioning during partial melting. Earth and Planetary Science Letters 307, 395–408.

Lee, C.-T.A., Anderson, D.L., 2015. Continental crust formation at arcs, the arclogite "delamination" cycle, and one origin for fertile melting anomalies in the mantle. Science Bulletin 60, 1141–1156.

Lissenberg, C.J., MacLeod, C.J., 2016. A reactive porous flow control on mid-ocean ridge magmatic evolution. Journal of Petrology 57, 2195–2220.

Lissenberg, C.J., MacLeod, C.J., Howard, K.A., Godard, M., 2013. Pervasive reactive melt migration through fast-spreading lower oceanic crust (Hess Deep, equatorial Pacific Ocean). Earth and Planetary Science Letters 361.

Liu, B., Liang, Y., 2017. The prevalence of kilometer-scale heterogeneity in the source region of MORB upper mantle. Science Advances 3, e1701872.

Liu, C.Z., Snow, J.E., Hellebrand, E., Brugmann, G., von der Handt, A., Buchl, A., Hofmann, A.W., 2008. Ancient, highly heterogeneous mantle beneath Gakkel ridge, Arctic Ocean. Nature 452, 311–316.

Lundstrom, C., 2000. Models of U-series disequilibria generation in MORB: the effects of two scales of melt porosity. Physics of the Earth and Planetary Interiors 121, 189–204.

Lundstrom, C.C., 2003. Uranium-series disequilibria in mid-ocean ridge basalts: observations and models of basalt genesis. Uranium-Series Geochemistry 52, 175–214.

Lundstrom, C.C., Gill, J., Williams, Q., Perfit, M.R., 1995. Mantle melting and basalt extraction by equilibrium porous flow. Science 270, 1958–1961.

Lundstrom, C.C., Gill, J., Williams, Q., Hanan, B.B., 1998a. Investigating solid mantle upwelling beneath mid-ocean ridges using U-series disequilibria. II. A local study at 33 degrees Mid-Atlantic Ridge. Earth and Planetary Science Letters 157, 167–181.

Lundstrom, C.C., Williams, Q., Gill, J.B., 1998b. Investigating solid mantle upwelling rates beneath mid-ocean ridges using U-series disequilibria, 1: a global approach. Earth and Planetary Science Letters 157, 151–165.

Lundstrom, C.C., Sampson, D.E., Perfit, M.R., Gill, J., Williams, Q., 1999. Insights into mid-ocean ridge basalt petrogenesis: U-series disequilibria from the Siqueiros Transform, Lamont Seamounts, and East Pacific Rise. Journal of Geophysical Research - Solid Earth 104, 13035–13048.

Lundstrom, C., Gill, J., Williams, Q., 2000. A geochemically consistent hypothesis for MORB generation. Chemical Geology 162, 105–126.

Lundstrom, C.C., Hoernle, K., Gill, J., 2003. U-series disequilibria in volcanic rocks from the Canary Islands: plume versus lithospheric melting. Geochimica et Cosmochimica Acta 67, 4153–4177.

Maclennan, J., 2008. Concurrent mixing and cooling of melts under Iceland. Journal of Petrology 49, 1931–1953.

Mallik, A., Dasgupta, R., 2012. Reaction between MORB-eclogite derived melts and fertile peridotite and generation of ocean island basalts. Earth and Planetary Science Letters 329-330, 97–108.

Matzen, A.K., Wood, B.J., Baker, M.B., Stolper, E.M., 2017. The roles of pyroxenite and peridotite in the mantle sources of oceanic basalts. Nature Geoscience 10, 530–535.

McDonough, W.F., 1991. Partial melting of subducted oceanic crust and isolation of its residual eclogitic lithology. Philosophical Transactions: Physical Sciences and Engineering 335, 407–418.

McKenzie, D., 1985. Th-230-U-238 disequilibrium and the melting processes beneath Ridge Axes. Earth and Planetary Science Letters 72, 149–157.

Medaris, L., Beard, B.L., Johnson, C.M., Valley, J.W., Spicuzza, M.J., Jelinek, E., Misar, Z., 1995. Garnet pyroxenite and eclogite in the Bohemian Massif: geochemical evidence for Variscan recycling of subducted lithosphere. Geologische Rundschau 84, 489–505.

Millet, M.A., Doucelance, R., Schiano, P., David, K., Bosq, C., 2008. Mantle plume heterogeneity versus shallow-level interactions: a case study, the São Nicolau Island, Cape Verde archipelago. Journal of Volcanology and Geothermal Research 176, 265–276.

Natland, J.H., 1989. Partial melting of a lithologically heterogeneous mantle: inferences from crystallization histories of magnesian abyssal tholeiites from the Siqueiros Fracture Zone. Geological Society, London, Special Publications 42, 41–70.

Navon, O., Stolper, E., 1987. Geochemical consequences of melt percolation: the upper mantle as a chromatographic column. The Journal of Geology 95, 285–307.

Niu, Y., Wilson, M., Humphreys, E.R., O'hara, M.J., 2011. The origin of intra-plate ocean island basalts (OIB): the lid effect and its geodynamic implications. Journal of Petrology 52, 1443–1468.

O'Hara, M., 1977. Geochemical evolution during fractional crystallisation of a periodically refilled magma chamber. Nature 266, 503–507.

Olson, P., 1988. Fate of subducted lithosphere. Nature 331, 113–114.

O'Neill, H.S.-C., Jenner, F.E., 2012. The global pattern of trace-element distributions in ocean floor basalts. Nature 491, 698–704.

Peate, D.W., Hawkesworth, C.J., van Calsteren, P.W., Taylor, R.N., Murton, B.J., 2001. U-238-Th-230 constraints on mantle upwelling and plume-ridge interaction along the Reykjanes Ridge. Earth and Planetary Science Letters 187, 259–272.

Pertermann, M., Hirschmann, M., 2003a. Partial melting experiments on MORB-like pyroxenite between 2 and 3 GPa: constraints on the presence of pyroxenite in basalt source regions from solidus location and melting rate. Journal of Geophysical Research 108. https://doi.org/10.1029/2000JB000118.

Pertermann, M., Hirschmann, M.M., 2003b. Anhydrous partial melting experiments on MORB-like eclogite: Phase relations, phase compositions and mineral-melt partitioning of major elements at 2-3 GPa. Journal of Petrology 44, 2173–2201.

Pertermann, M., Hirschmann, M.M., Hametner, K., Gunther, D., Schmidt, M.W., 2004. Experimental determination of trace element partitioning between garnet and silica-rich liquid during anhydrous partial melting of MORB-like eclogite. Geochemistry, Geophysics, Geosystems 5 (Q05A01).

Phillips, E.H., Sims, K.W., Sherrod, D.R., Salters, V.J., Blusztajn, J., Dulai, H., 2016. Isotopic constraints on the genesis and evolution of basanitic lavas at Haleakala, Island of Maui, Hawaii. Geochimica et Cosmochimica Acta 195, 201–225.

Phipps Morgan, J., 2001. Thermodynamics of pressure release melting of a veined plum pudding mantle. Geochemistry, Geophysics, Geosystems 2 (10.1029/2000GC000049).

Pickett, D.A., Murrell, M.T., 1997. Observations of (^{231}Pa)/(^{235}U) disequilibrium in volcanic rocks. Earth and Planetary Science Letters 148, 259–271.

Pietruszka, A.J., Rubin, K.H., Garcia, M.O., 2001. Ra-226-Th-230-U-238 disequilibria of historical Kilauea lavas (1790-1982) and the dynamics of mantle melting within the Hawaiian plume. Earth and Planetary Science Letters 186, 15–31.

Pietruszka, A.J., Hauri, E.H., Blichert-Toft, J., 2009. Crustal contamination of mantle-derived magmas within Piton de la Fournaise Volcano, Réunion Island. Journal of Petrology 50, 661–684.

Prinzhofer, A., Lewin, E., Allegre, C., 1989. Stochastic melting of the marble cake mantle: evidence from local study of the East Pacific Rise at 12 50′ N. Earth and Planetary Science Letters 92, 189–206.

Prytulak, J., Elliott, T., 2007. TiO_2 enrichment in ocean island basalts. Earth and Planetary Science Letters 263, 388–403.

Prytulak, J., Elliott, T., 2009. Determining melt productivity of mantle sources from U-238-Th-230 and U-235-Pa-231 disequilibria; an example from Pico Island, Azores. Geochimica et Cosmochimica Acta 73, 2103–2122.

Prytulak, J., Avanzinelli, R., Koetsier, G., Kreissig, K., Beier, C., Elliott, T., 2014. Melting versus contamination effects on ^{238}U-^{230}Th-^{226}Ra and ^{235}U-^{231}Pa disequilibria in lavas from São Miguel, Azores. Chemical Geology 381, 94–109.

Qin, L., Humayun, M., 2008. The Fe/Mn ratio in MORB and OIB determined by ICP-MS. Geochimica et Cosmochimica Acta 72, 1660–1677.

Rampone, E., Borghini, G., 2008. Melt migration and intrusion in the Erro-Tobbio peridotites (Ligurian Alps, Italy): Insights on magmatic processes in extending lithospheric mantle. European Journal of Mineralogy 20, 573–585.

Rampone, E., Hofmann, A.W., 2012. A global overview of isotopic heterogeneities in the oceanic mantle. Lithos 148, 247–261.

Reagan, M., Turner, S., Handley, H., Turner, M., Beier, C., Caulfield, J., Peate, D., 2017. ^{210}Pb-^{226}Ra disequilibria in young gas-laden magmas. Scientific Reports 7, 45186.

Ribe, N.M., 1985. The generation and composition of partial melts in the earth's mantle. Earth and Planetary Science Letters 73, 361–376.

Ribe, N.M., 1988. Dynamical geochemistry of the Hawaiian plume. Earth and Planetary Science Letters 88, 37–46.

Richardson, C., McKenzie, D., 1994. Radioactive disequilibria from 2D models of melt generation by plumes and ridges. Earth and Planetary Science Letters 128, 425–437.

Rosenthal, A., Yaxley, G.M., Green, D.H., Hermann, J., Kovácz, I., Spandler, C., 2014. Continuous eclogite melting and variable refertilisation in upwelling heterogeneous mantle. Scientific Reports 4, 6099.

Rosenthal, A., Yaxley, G.M., Crichton, W.A., Kovacs, I., Spandler, C., Hermann, J., Pelleter, A.A., 2018. Phase relations and melting of nominally 'dry'residual eclogites with variable CaO/Na_2O from 3 to 5 GPa and 1250 to 1500° C; implications for refertilisation of upwelling heterogeneous mantle. Lithos. 314-315, 506–519. https://www.sciencedirect.com/science/article/pii/S0024493718301889.

Rubin, K., Macdougall, J., 1992. Th-Sr isotopic relationships in MORB. Earth and Planetary Science Letters 114, 149–157.

Rubin, K.H., van der Zander, I., Smith, M.C., Bergmanis, E.C., 2005. Minimum speed limit for ocean ridge magmatism from Pb-210-Ra-226-Th-230 disequilibria. Nature 437, 534–538.

Rubin, K.H., Sinton, J.M., Maclennan, J., Hellebrand, E., 2009. Magmatic filtering of mantle compositions at mid-ocean-ridge volcanoes. Nature Geoscience 2, 321–328.

Rudge, J.F., Maclennan, J., Stracke, A., 2013. The geochemical consequences of mixing melts from a heterogeneous mantle. Geochimica et Cosmochimica Acta 114, 112–143.

Russo, C.J., Rubin, K.H., Graham, D.W., 2009. Mantle melting and magma supply to the Southeast Indian Ridge: The roles of lithology and melting conditions from U-series disequilibria. Earth and Planetary Science Letters 278, 55–66.

Saal, A.E., Van Orman, J.A., 2004. The Ra-226 enrichment in oceanic basalts: Evidence for melt-cumulate diffusive interaction processes within the oceanic lithosphere. Geochemistry, Geophysics, Geosystems 5. https://doi.org/10.1029/2003GC000620.
Salters, V.J., Dick, H.J., 2002. Mineralogy of the mid-ocean-ridge basalt source from neodymium isotopic composition of abyssal peridotites. Nature 418, 68–72.
Salters, V.J.M., Longhi, J., 1999. Trace element partitioning during the initial stages of melting beneath mid-ocean ridges. Earth and Planetary Science Letters 166, 15–30.
Salters, V.J., Stracke, A., 2004. Composition of the depleted mantle. Geochemistry, Geophysics, Geosystems 5. https://doi.org/10.1029/2003GC000597.
Salters, V.J.M., Longhi, J.E., Bizimis, M., 2002. Near mantle solidus trace element partitioning at pressures up to 3.4 GPa. Geochemistry, Geophysics, Geosystems 3, 1038. https://doi.org/10.1029/2001GC000148.
Schiano, P., Birck, J.L., Allègre, C.J., 1997. Osmium-strontium-neodymium-lead isotopic covariations in mid-ocean ridge basalt glasses and the heterogeneity of the upper mantle. Earth and Planetary Science Letters 150, 363–379.
Seyler, M., Lorand, J.-P., Dick, H.J., Drouin, M., 2007. Pervasive melt percolation reactions in ultra-depleted refractory harzburgites at the Mid-Atlantic Ridge, 15 20′ N: ODP Hole 1274A. Contributions to Mineralogy and Petrology 153, 303. https://doi.org/10.1007/s00410-006-0148-6.
Shorttle, O., Maclennan, J., 2011. Compositional trends of Icelandic basalts: Implications for short-length scale lithological heterogeneity in mantle plumes. Geochemistry, Geophysics, Geosystems 12. https://doi.org/10.1029/2011GC003748.
Shorttle, O., Maclennan, J., Lambart, S., 2014. Quantifying lithological variability in the mantle. Earth and Planetary Science Letters 395, 24–40.
Sigmarsson, O., Steinthórsson, S., 2007. Origin of Icelandic basalts: A review of their petrology and geochemistry. Journal of Geodynamics 43, 87–100.
Sigmarsson, O., Carn, S., Carracedo, J.C., 1998. Systematics of U-series nuclides in primitive lavas from the 1730-36 eruption on Lanzarote, Canary Islands, and implications for the role of garnet pyroxenites during oceanic basalt formations. Earth and Planetary Science Letters 162, 137–151.
Sims, K.W.W., Hart, S.R., 2006. Comparison of Th, Sr, Nd and Pb isotopes in oceanic basalts: Implications for mantle heterogeneity and magma genesis. Earth and Planetary Science Letters 245, 743–761.
Sims, K.W.W., Depaolo, D.J., Murrell, M.T., Baldridge, W.S., Goldstein, S.J., Clague, D.A., 1995. Mechanisms of Magma Generation beneath Hawaii and Midocean Ridges - Uranium/Thorium and Samarium/Neodymium Isotopic Evidence. Science 267, 508–512.
Sims, K.W.W., DePaolo, D.J., Murrell, M.T., Baldridge, W.S., Goldstein, S., Clague, D., Jull, M., 1999. Porosity of the melting zone and variations in the solid mantle upwelling rate beneath Hawaii: Inferences from U-238-Th-230-Ra-226 and U-235-Pa-231 disequilibria. Geochimica et Cosmochimica Acta 63, 4119–4138.
Sims, K.W.W., Goldstein, S.J., Blichert-Toft, J., Perfit, M.R., Kelemen, P., Fornari, D.J., Michael, P., Murrell, M.T., Hart, S.R., DePaolo, D.J., Layne, G., Ball, L., Jull, M., Bender, J., 2002. Chemical and isotopic constraints on the generation and transport of magma beneath the East Pacific Rise. Geochimica et Cosmochimica Acta 66, 3481–3504.
Sims, K.W.W., Blichert-Toft, J., Fornari, D.J., Perfit, M.R., Goldstein, S.J., Johnson, P., DePaolo, D.J., Hart, S.R., Murrell, P.J., Michael, P.J., Layne, G.D., Ball, L.A., 2003. Aberrant youth: Chemical and isotopic constraints on the origin of off-axis lavas from the East Pacific Rise, 9 degrees-10 degrees N. Geochemistry, Geophysics, Geosystems 4, 8621.
Sims, K.W.W., Hart, S.R., Reagan, M.K., Blusztajn, J., Staudigel, H., Sohn, R.A., Layne, G.D., Ball, L.A., 2008. ^{238}U-^{230}Th-^{226}Ra-^{210}Pb-^{210}Po, ^{232}Th-^{228}Ra, and ^{235}U-^{231}Pa constraints on the ages and petrogenesis of Vailulu'u and Malumalu Lavas, Samoa. Geochemistry, Geophysics, Geosystems 9 Q04003.
Sims, K.W.W., Maclennan, J., Blichert-Toft, J., Mervine, E.M., Blusztajn, J., Grönvold, K., 2013. Short length scale mantle heterogeneity beneath Iceland probed by glacial modulation of melting. Earth and Planetary Science Letters 379, 146–157.
Sleep, N., 1984. Tapping of magmas from ubiquitous mantle heterogeneities: An alternative to mantle plumes? Journal of Geophysical Research - Solid Earth 89, 10029–10041.
Smith, P.M., Asimow, P.D., 2005. Adiabat_1ph: A new public front-end to the MELTS, pMELTS, and pHMELTS models. Geochemistry, Geophysics, Geosystems 6. https://doi.org/10.1029/2004GC000816.
Sobolev, A.V., Hofmann, A.W., Sobolev, S.V., Nikogosian, I.K., 2005. An olivine-free mantle source of Hawaiian shield basalts. Nature 434, 590.
Sobolev, A.V., Hofmann, A.W., Kuzmin, D.V., Yaxley, G.M., Arndt, N.T., Chung, S.-L., Danyushevsky, L.V., Elliott, T., Frey, F.A., Garcia, M.O., 2007. The amount of recycled crust in sources of mantle-derived melts. Science 316, 412–417.
Sobolev, A.V., Hofmann, A.W., Brügmann, G., Batanova, V.G., Kuzmin, D.V., 2008. A quantitative link between recycling and osmium isotopes. Science 321, 536.
Spandler, C., Hammerli, J., Yaxley, G.M., 2017. An experimental study of trace element distribution during partial melting of mantle heterogeneities. Chemical Geology 462, 74–87.
Spiegelman, M., 2000. UserCalc: a web-based uranium series calculator for magma migration problems. Geochemistry, Geophysics, Geosystems 1, 1016.
Spiegelman, M., Elliott, T., 1993. Consequences of Melt Transport for Uranium Series Disequilibrium in Young Lavas. Earth and Planetary Science Letters 118, 1–20.
Spiegelman, M., Kelemen, P.B., 2003. Extreme chemical variability as a consequence of channelized melt transport. Geochemistry, Geophysics, Geosystems 4, 1055.
Spiegelman, M., Kenyon, P., 1992. The requirements for chemical disequilibrium during magma migration. Earth and Planetary Science Letters 109, 611–620.
Spiegelman, M., Kelemen, P., Aharonov, E., 2001. Causes and consequences of flow organization during melt transport: the reaction infiltration instability in compactible media. Journal of Geophysical Research - Solid Earth 106, 2061–2077.
Standish, J.J., Sims, K.W.W., 2010. Young off-axis volcanism along the ultraslow-spreading Southwest Indian Ridge. Nature Geoscience 3, 286–292.
Stolper, E.M., Asimow, P.D., 2007. Insights into mantle melting from graphical analysis of one-component systems. American Journal of Science 307, 1051–1139.
Stracke, A., Bourdon, B., 2009. The importance of melt extraction for tracing mantle heterogeneities. Geochimica et Cosmochimica Acta 73, 218–238.
Stracke, A., Salters, V.J.M., Sims, K.W.W., 1999. Assessing the presence of garnet-pyroxenite in the mantle sources of basalts through combined hafnium-neodymium-thorium isotope systematics. Geochemistry, Geophysics, Geosystems, 1 https://doi.org/10.1029/1999GC000013.
Stracke, A., Bizimis, M., Salters, V.J.M., 2003a. Recycling oceanic crust: Quantitative constraints. Geochemistry, Geophysics, Geosystems 4, 8003.
Stracke, A., Zindler, A., Salters, V.J.M., McKenzie, D., Blichert-Toft, J., Albarede, F., Gronvold, K., 2003b. Theistareykir revisited. Geochemistry, Geophysics, Geosystems 4. https://doi.org/10.1029/2001GC000201.
Stracke, A., Zindler, A., Salters, V.J.M., McKenzie, D., Gronvold, K., 2003c. The dynamics of melting beneath Theistareykir, northern Iceland. Geochemistry, Geophysics, Geosystems 4, 8513.
Stracke, A., Bourdon, B., McKenzie, D., 2006. Melt extraction in the Earth's mantle: constraints from U-Th-Pa-Ra studies in oceanic basalts. Earth and Planetary Science Letters 244, 97–112.
Tepley, F.J., Lundstrom, C.C., Sims, K.W.W., Hekinian, R., 2004. U-series disequilibria in MORB from the Garrett Transform and implications for mantle melting. Earth and Planetary Science Letters 223, 79–97.
Turner, S., Hawkesworth, C., Rogers, N., King, P., 1997. U-Th isotope disequilibria and ocean island basalt generation in the Azores. Chemical Geology 139, 145–164.
Turner, S., Bourdon, B., Hawkesworth, C., Evans, P., 2000. 226 Ra–230 Th evidence for multiple dehydration events, rapid melt ascent and the time scales of differentiation beneath the Tonga–Kermadec island arc. Earth and Planetary Science Letters 179, 581–593.
Turner, S., Kokfelt, T., Hauff, F., Haase, K., Lundstrom, C., Hoernle, K., Yeo, I.A., Devey, C., 2015. Mid-ocean ridge basalt generation along the slow-spreading, South Mid-Atlantic Ridge (5-11°S): Inferences from ^{238}U-^{230}Th-^{226}Ra disequilibria. Geochimica et Cosmochimica Acta 169, 152–166.
Turner, S., Kokfelt, T., Hoernle, K., Lundstrom, C., Hauff, F., 2016. ^{231}Pa systematics in postglacial volcanic rocks from Iceland. Geochimica et Cosmochimica Acta 185, 129–140.
Turner, S., Kokfelt, T., Hoernle, K., Johansen, T., Hauff, F., Lundstrom, C., van den Bogaard, P., Klügel, A., 2017. Contrasting magmatic cannibalism forms evolved phonolitic magmas in the Canary Islands. Geology 45, 147–150.
Varas-Reus, M.I., Garrido, C.J., Marchesi, C., Bosch, D., Hidas, K., 2018. Genesis of ultra-high pressure garnet pyroxenites in orogenic peridotites and its bearing on the compositional heterogeneity of the Earth's mantle. Geochimica et Cosmochimica Acta 232, 303–328.
Warren, J.M., 2016. Global variations in abyssal peridotite compositions. Lithos 248-251, 193–219.
Warren, J., Shirey, S., 2012. Lead and osmium isotopic constraints on the oceanic mantle from single abyssal peridotite sulfides. Earth and Planetary Science Letters 359, 279–293.
Warren, J.M., Shimizu, N., Sakaguchi, C., Dick, H.J.B., Nakamura, E., 2009. An assessment of upper mantle heterogeneity based on abyssal peridotite isotopic compositions. Journal of Geophysical Research B114, B12203.
Waters, C.L., Sims, K.W.W., Perfit, M.R., Blichert-Toft, J., Blusztajn, J., 2011. Perspective on the genesis of E-MORB from chemical and isotopic heterogeneity at 9°-10°N East Pacific Rise. Journal of Petrology 52, 565–602.
Waters, C.L., Sims, K.W.W., Klein, E.M., White, S.M., Reagan, M.K., Girard, G., 2013. Sill to surface: Linking young off-axis volcanism with subsurface melt at the overlapping spreading center at 9°03'N East Pacific Rise. Earth and Planetary Science Letters 369-370, 59–70.
Weatherley, S.M., Katz, R.F., 2012. Melting and channelized magmatic flow in chemically heterogeneous, upwelling mantle. Geochemistry, Geophysics, Geosystems 13 (Q0AC18).
Weatherley, S.M., Katz, R.F., 2016. Melt transport rates in heterogeneous mantle beneath mid-ocean ridges. Geochimica et Cosmochimica Acta 172, 39–54.
White, W., Hofmann, A., 1982. Sr and Nd isotope geochemistry of oceanic basalts and mantle evolution. Nature 296, 821–825.
Williams, R.W., Gill, J.B., 1989. Effects of partial melting on the uranium decay series. Geochimica et Cosmochimica Acta 53, 1607–1619.
Xu, Y., 2002. Evidence for crustal components in the mantle and constraints on crustal recycling mechanisms: pyroxenite xenoliths from Hannuoba, North China. Chemical Geology 182, 301–322.
Yaxley, G.M., Green, D.H., 1998. Reactions between eclogite and peridotite: mantle refertilisation by subduction of oceanic crust. Schweizerische Mineralogische und Petrographische Mitteilungen 78, 243–255.
Yaxley, G., Sobolev, A.V., 2007. High-pressure partial melting of gabbro and its role in the Hawaiian magma source. Contributions to Mineralogy and Petrology 154, 371–383.
Zhang, G.L., Zong, C.L., Yin, X.B., Li, H., 2012. Geochemical constraints on a mixed pyroxenite–peridotite source for East Pacific Rise basalts. Chemical Geology 330, 176–187.
Zindler, A., Staudigel, H., Batiza, R., 1984. Isotope and trace element geochemistry of young Pacific seamounts: implications for the scale of upper mantle heterogeneity. Earth and Planetary Science Letters 70, 175–195.
Zou, H.B., Zindler, A., 2000. Theoretical studies of U-238-Th-230-Ra-226 and U-235-Pa-231 disequilibria in young lavas produced by mantle melting. Geochimica et Cosmochimica Acta 64, 1809–1817.

Update

LITHOS

Volume 452–453, Issue , September 2023, Page

DOI: https://doi.org/10.1016/j.lithos.2023.107217

LITHOS 452–453 (2023) 107217

Contents lists available at ScienceDirect

LITHOS

journal homepage: www.elsevier.com/locate/lithos

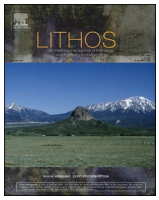

Corrigendum to "Testing pyroxenite versus peridotite sources for marine basalts using U-series isotopes" [Lithos 332–333 (2019) 226–244]

Lynne J. Elkins [a,*], Bernard Bourdon [b], Sarah Lambart [c]

[a] University of Nebraska-Lincoln, Lincoln, NE, USA
[b] Ecole Normale Supérieure de Lyon, CNRS, UCBL, Université de Lyon, Lyon, France
[c] University of Utah, Salt Lake City, UT, USA

The authors regret that a small error in the dynamic melting Matlab script used for this paper produced erroneous results for some of the included modeling outcomes. We have written an updated modeling program in python, which can be accessed in the ENKI and pyUserCalc public data repository (https://gitlab.com/ENKI-portal/pyUsercalc/). Although the corrected results shown in revised versions of Figs. S3, S4, S8, S9, and S10 now appear quite different from the original publication, however, we find that when restricted to plausible scenarios of interest, our conclusions overall have not significantly changed. Some details of our results and discussion require corrections, however.

5.2.5. Modeling outcomes

Corrected dynamic melting outcomes for peridotite melting are significantly expanded in (^{230}Th/^{238}U) from earlier results, particularly for high potential temperatures. At $T_p = 1300$ °C, corrected (^{230}Th/^{238}U) activity ratios extend from moderately low values (i.e., up to 5% ^{230}Th deficits relative to ^{238}U) to small (~5%) ^{230}Th excesses, depending primarily on the solid mantle upwelling rate. The more significant differences from our prior results occur at $T_p = 1550$ °C, where the full range of (^{230}Th/^{238}U) now extends from 0.7 to 1.4. The most extreme high values (greater than 1.1) are limited to scenarios with solid mantle upwelling rates slower than 5 cm/yr., however, which may be less realistic in high-temperature settings. The notably large ^{230}Th *deficits* occur at particularly rapid upwelling rates of 20 and 50 cm/yr and low reference porosities, and may be a product of continued melting in the spinel stability field.

Corrected peridotite (^{226}Ra/^{230}Th) results at $T_p = 1300$ °C span overall ranges of 1.2 to 3.6, and (^{231}Pa/^{235}U) from 0.4 to 3.2, though we note that such low values (^{231}Pa deficits) are probably not plausible outcomes. These unlikely deficits occurred only for particularly small residual porosities (0.1–0.2%) coupled with very fast upwelling (20 to 50 cm/yr.) and may indicate a model artifact when solving for especially low Pa concentrations. At higher temperatures of $T_p = 1550$ °C, (^{226}Ra/^{230}Th) ranges from 1.4 to 5.6, while (^{231}Pa/^{235}U) again ranges from levels as low as 0.3 to 6.2.

Our corrected dynamic melting outcomes for pyroxenite partial melts are also different from earlier outcomes. The biggest change is that (^{230}Th/^{238}U) disequilibria are generally lower for conditions of interest than previously calculated (Fig. 7), although the span of outcomes across all tested conditions is still quite broad. We find that at $T_p = 1300$ °C, (^{230}Th/^{238}U) in Gb108 partial melts ranges from 0.75 to 1.7, and at $T_p = 1550$ °C, the range is from 0.45 to 2.5. For MIX1G, the ranges are 0.9 to 1.3 at 1300 °C and 0.8 to 1.5 at 1550 °C. Most (^{226}Ra/^{230}Th) and (^{231}Pa/^{235}U) ratios in pyroxenite melts are significantly higher than peridotite melts, though overall, results for MIX1G more closely resemble peridotite melts than those for Gb108 at high temperatures.

Interestingly, while most outcomes are similar between thermal equilibrium and thermally isolated conditions between pyroxenite and peridotite, we do observe notably different outcomes for Gb108 partial melts at 1550 °C, such that the ranges of disequilibria are significantly expanded when thermally isolated (Fig. S10), compared to thermally equilibrated conditions (Fig. S4).

6. Discussion

Many of our revised results for peridotite melting now more closely align with prior studies than our previous results. Some of our corrected results for dynamic melting of both peridotite and pyroxenite also now better reproduce the compositions observed in global MORB. However, when those outcomes are restricted to plausible scenarios for mid-ocean ridge and ocean island melting environments (e.g., faster upwelling at most hotspot settings than beneath passively upwelling divergent regions), the resulting ranges are more restricted than the full revised results shown in Figs. S3, S4, S8, S9, and S10 initially suggest. Thus, while our corrected outcomes better align with prior results, we find that they do not significantly change our overall conclusions.

Fig. 7 shows a revised summary of melting outcomes for conditions of interest in both mid-ocean ridge and ocean island settings, similar to the original figure. To more fully contextualize the corrected model outcomes, we now include results for all tested lithologies from both the dynamic and RPF (reactive porous flow) melting models. For upwelling rates of interest, the corrected dynamic melting outcomes for both peridotites and pyroxenites can still explain many observed compositions

DOI of original article: https://doi.org/10.1016/j.lithos.2019.02.011.
* Corresponding author.
E-mail address: lelkins@unl.edu (L.J. Elkins).

https://doi.org/10.1016/j.lithos.2023.107217

Available online 25 May 2023

of global MORBs and OIBs. That said, the dynamic melts of pyroxenites are restricted to somewhat lower (^{230}Th/^{238}U) for plausible upwelling rates and porosities, extending up to ~1.25 at the highest. At 1550 °C, only very slow upwelling could achieve higher ^{230}Th excesses, and the more plausible upwelling rates of 2–50 cm/yr exhibit much more restricted disequilibria, due to the shorter residence times of partial melts in the melting regime. While the revised dynamic melting ranges in Fig. 7 do overlap with much of the global data set, they cannot easily explain the most extreme high (^{230}Th/^{238}U) observed in some MORBs and OIBs, which may require other conditions.

We note that RPF melts of pyroxenite span a broader range than our revised dynamic melts. While RPF melts of pyroxenite also exhibit higher (^{226}Ra/^{230}Th) and (^{231}Pa/^{235}U) (Fig. 7), the summary data shown are restricted to lower porosity values for RPF scenarios. We suggest that the highest (^{230}Th/^{238}U) and lowest (^{226}Ra/^{230}Th) and (^{231}Pa/^{235}U) may be better explained by RPF melts with lower porosities, such that some enhanced chemical interaction during transport may occur under certain conditions. This finding strengthens our earlier conclusion that (1) some reactive flow and two-porosity transport may in fact be necessary to explain the full global U-series isotope systematics of oceanic basalts, even in heterogeneous melting regimes, and (2) that pyroxenite should be present in the source of OIB and MORB.

The authors would like to apologise for any inconvenience caused.

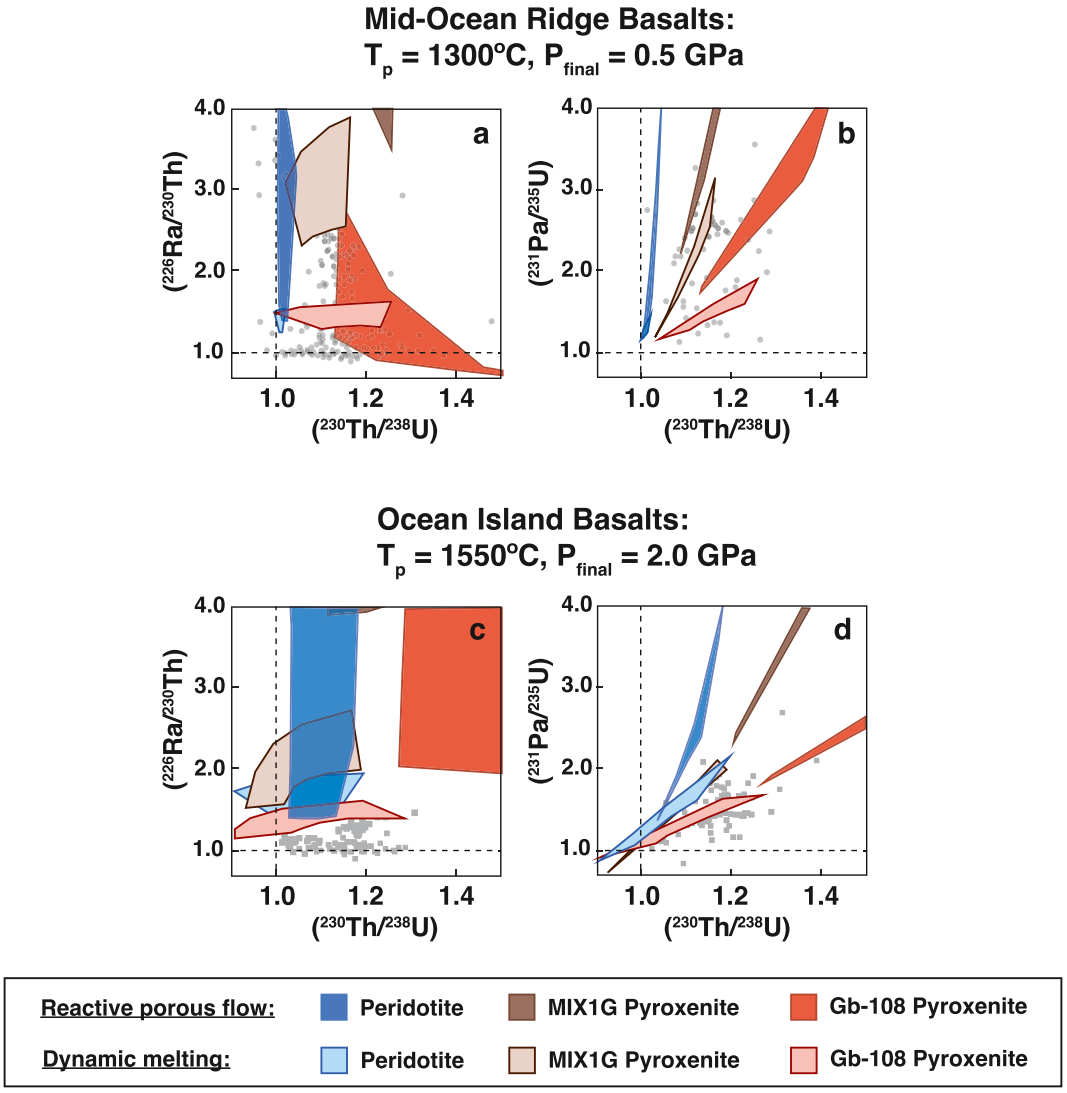

Fig. 7 Summary figure highlighting dynamic and RPF melt modeling calculation results of interest for peridotite and pyroxenite lithologies, after Fig. 7 in the original manuscript. In addition to corrected results for dynamic melting, this revised figure illustrates a more complete set of comparisons by including both dynamic melts of peridotite and RPF melts of pyroxenites. As in the original figure, dynamic melts are shown for residual porosities of 0.5 to 1.0%, while RPF melts are shown for maximum porosities of 0.1 to 0.5%, now for all lithologies. Mid-ocean ridge basalt modeling outcomes are shown for relevant solid mantle upwelling rates of 1 to 10 cm/yr, as in the original figure. Ocean island basalt modeling outcomes for pyroxenite have been expanded to include upwelling rates of 2 to 50 cm/yr for a more thorough comparison.

Fig. S3 Gridded results of time-dependent dynamic melting model calculations, for T_p = 1300 °C, final melting pressure of 0.5 GPa, and peridotite and pyroxenite in thermal equilibrium, across a range of solid mantle upwelling (W; solid lines) and maximum residual melt porosity (ϕ) values (dashed lines). Data fields indicate global MORB data after Fig. 3. Panels show results for **a.** (^{226}Ra/^{230}Th) and **b.** (^{231}Pa/^{235}U) vs. (^{230}Th/^{238}U) in partial melts of peridotite in thermal equilibrium with Gb-108 pyroxenite, **c.** (^{226}Ra/^{230}Th) and **d.** (^{231}Pa/^{235}U) vs.

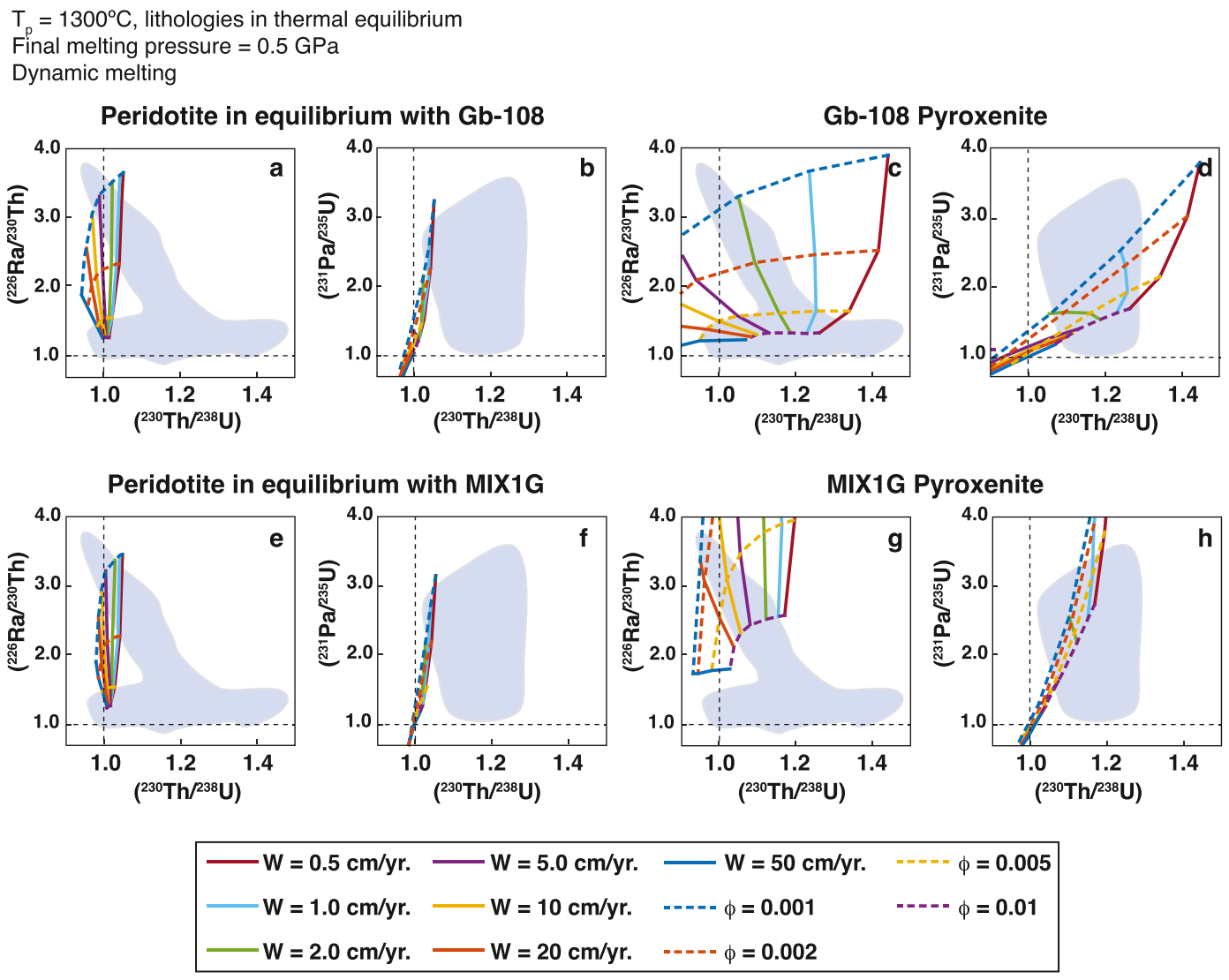

(^{230}Th/^{238}U) in partial melts of Gb-108 pyroxenite, **e.** (^{226}Ra/^{230}Th) and **f.** (^{231}Pa/^{235}U) vs. (^{230}Th/^{238}U) in partial melts of peridotite in thermal equilibrium with MIX-1G pyroxenite, and **g.** (^{226}Ra/^{230}Th) and **h.** (^{231}Pa/^{235}U) vs. (^{230}Th/^{238}U) in partial melts of MIX-1G pyroxenite. This figure has been updated to include revised dynamic melting results.

Fig. S4 Gridded results of time-dependent dynamic melting model calculations, for T_p = 1550 °C, final melting pressure of 0.5 GPa, and peridotite and pyroxenite in thermal equilibrium, across a range of solid mantle upwelling (W) and maximum residual melt porosity (ϕ) values and with panels as in Fig. S3. Data fields indicate global OIB data after Fig. 4. This figure has been updated to include revised dynamic melting results.

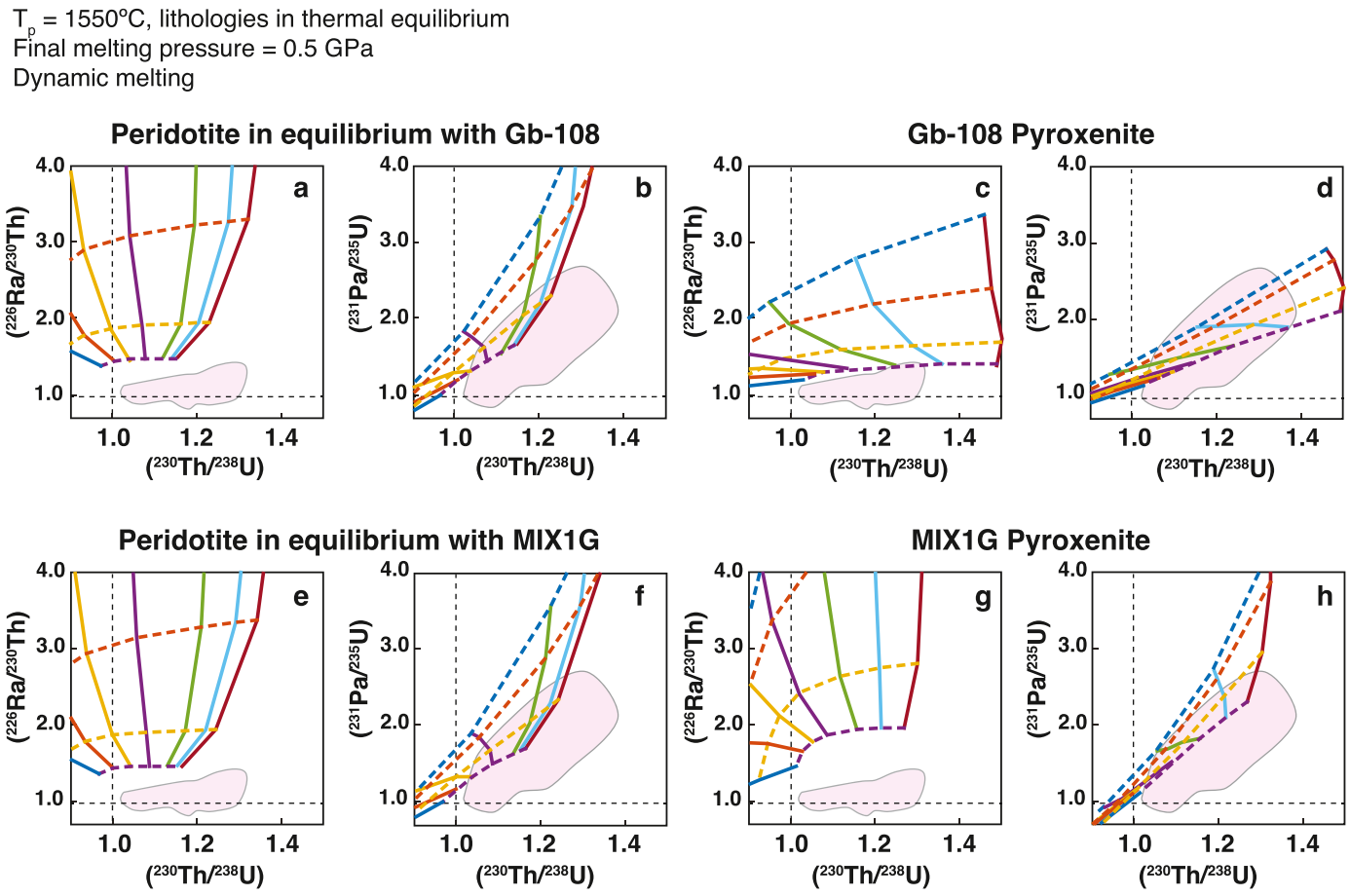

T_p = 1550°C, lithologies in thermal equilibrium
Final melting pressure = 2.0 GPa
Dynamic melting

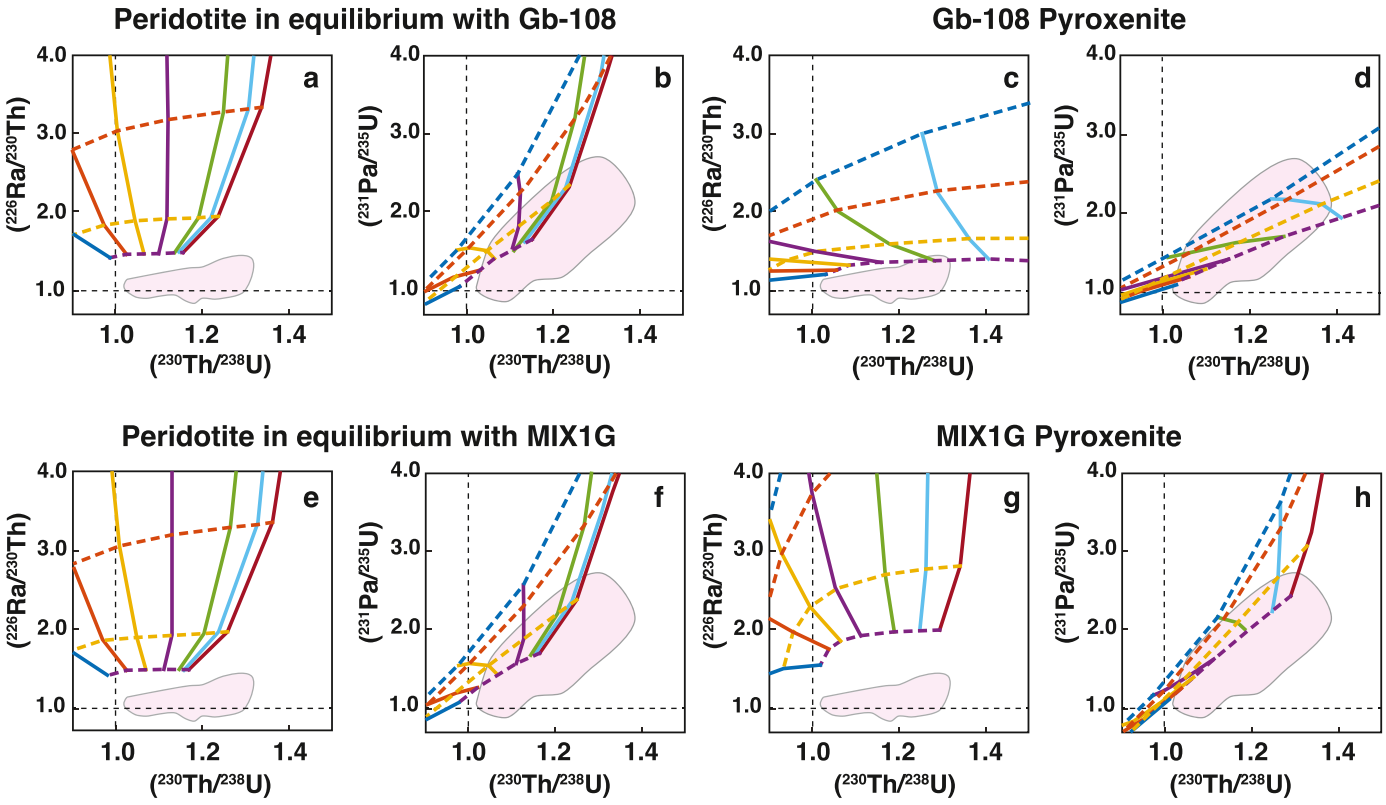

Fig. S8 Gridded results of time-dependent dynamic melting calculations, for $T_p = 1550$ °C, final melting pressure of 2.0 GPa, and peridotite and pyroxenite in thermal equilibrium, across a range of solid mantle upwelling (W) and maximum residual melt porosity (ϕ) values and with panels and fields as in Fig. S4. This figure has been updated to include revised dynamic melting results.

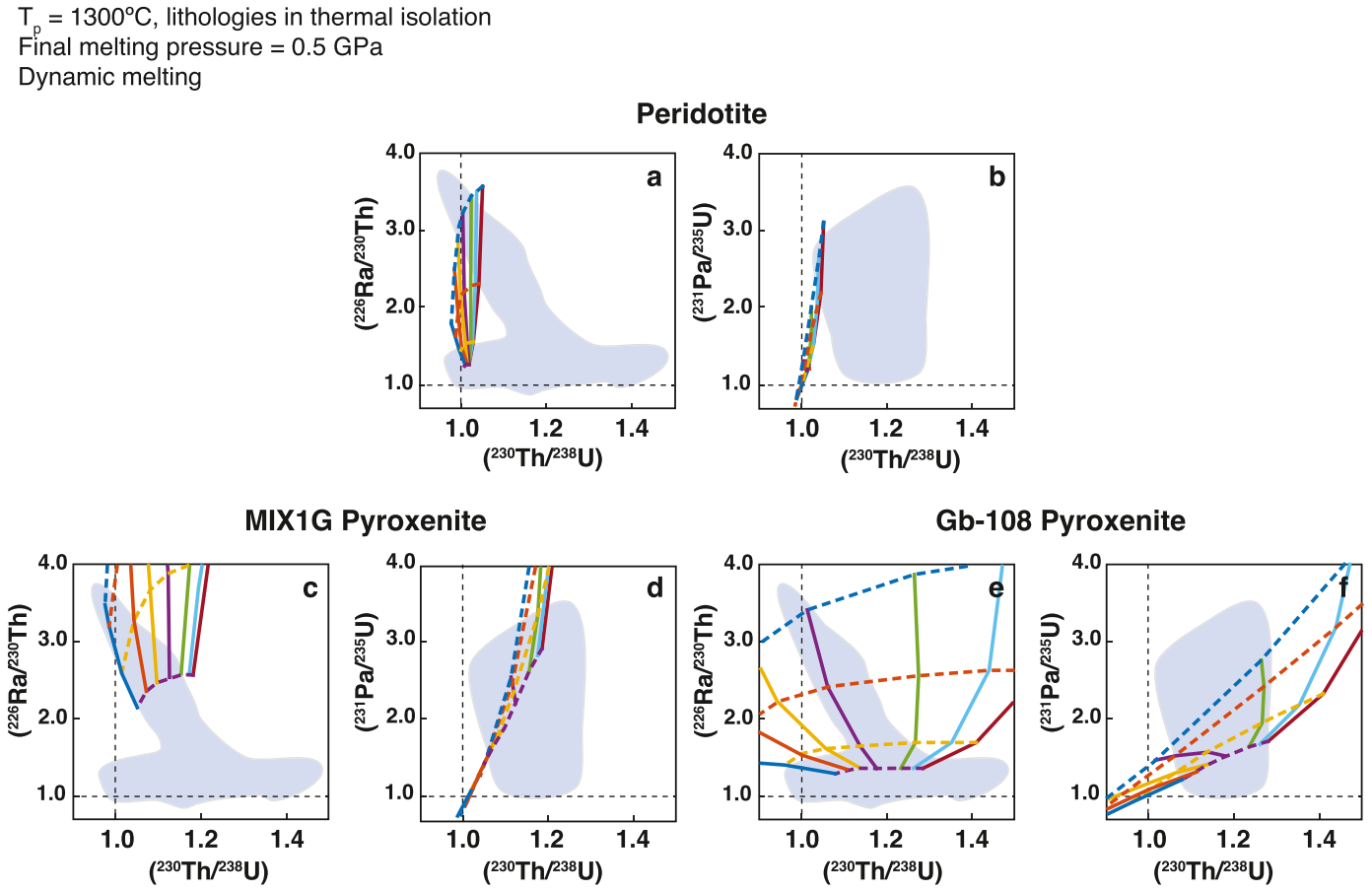

Fig. S9 Gridded results of time-dependent dynamic melting model calculations, for T_p = 1300 °C, final melting pressure of 0.5 GPa, and thermally isolated peridotite and pyroxenite, across a range of solid mantle upwelling (W) and maximum residual melt porosity (ϕ) values. Data fields are as in Fig. S3. Panels show results for **a.** (^{226}Ra/^{230}Th) and **b.** (^{231}Pa/^{235}U) vs. (^{230}Th/^{238}U) in partial melts of peridotite, **c.** (^{226}Ra/^{230}Th) and **d.** (^{231}Pa/^{235}U) vs. (^{230}Th/^{238}U) in partial melts of Gb-108 pyroxenite, and **e.** (^{226}Ra/^{230}Th) and **f.** (^{231}Pa/^{235}U) vs. (^{230}Th/^{238}U) in partial melts of MIX-1G pyroxenite. This figure has been updated to include revised dynamic melting results.

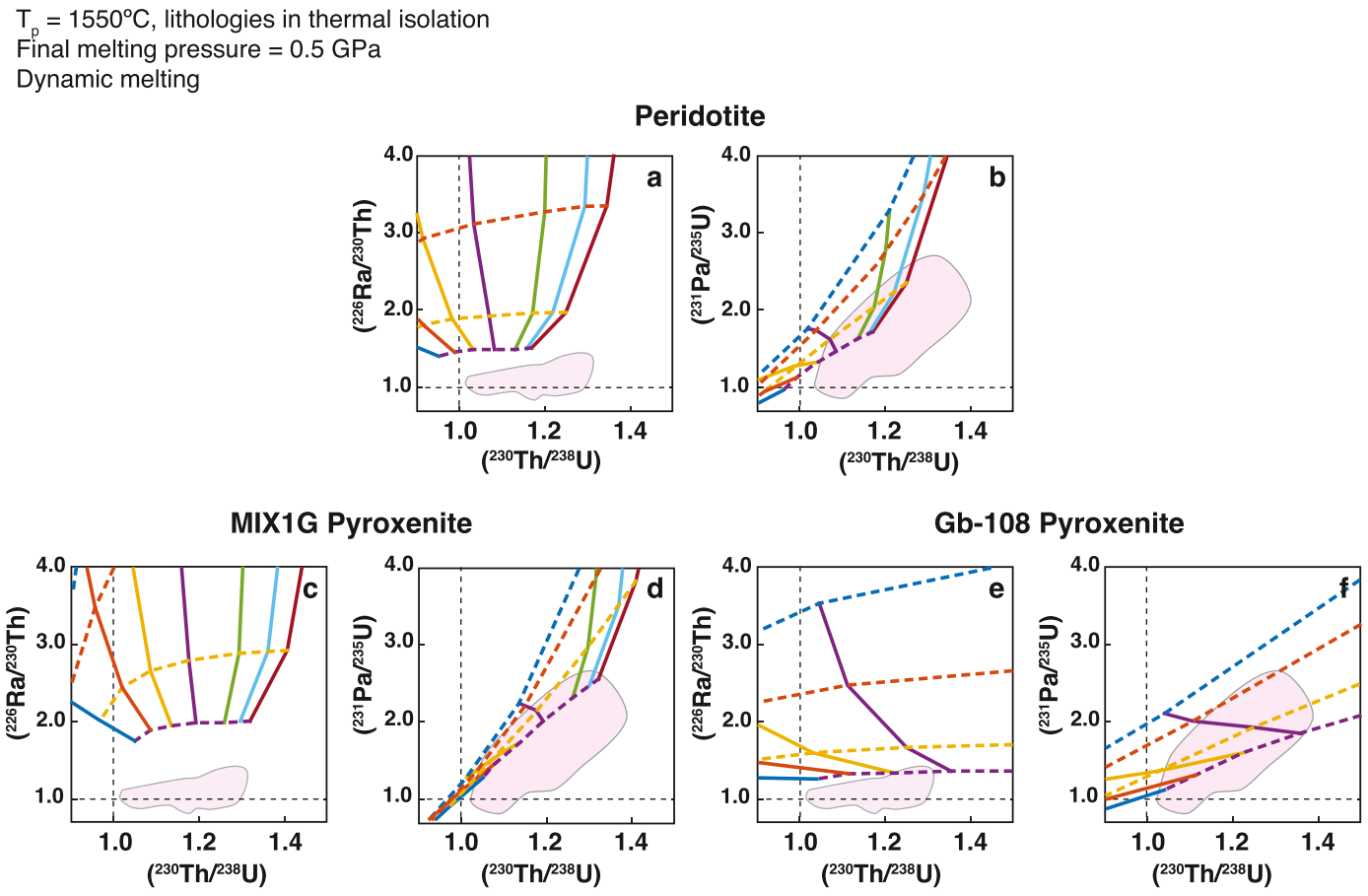

Fig. S10 Gridded results of time-dependent dynamic melting model calculations, for $T_p = 1550$ °C, final melting pressure of 0.5 GPa, and thermally isolated peridotite and pyroxenite, across a range of solid mantle upwelling (W) and maximum residual melt porosity (ϕ) values and with panels and fields as in Fig. S4. This figure has been updated to include revised dynamic melting results.